Gondwana break-up related magmatism in the Falkland Islands

Gondwana break-up related magmatism in the Falkland Islands

M. J. Hole[1], R.M. Ellam[2], D.I.M. MacDonald[1] & S.P. Kelley[3]

[1]*Department of Geology & Petroleum Geology University of Aberdeen, AB24 3UE, UK*
[2] *Scottish Universities Environment Research Centre, East Kilbride, Glasgow, G75 0QU, UK*
[3] *Department of Earth & Environmental Sciences, Open University, Milton Keynes, MK7 6AA* UK

Jurassic dykes (178-182 Ma) are widespread across the Falkland Islands and four distinct suites of intrusions are recognized. NW-SE oriented dykes have εNd_{182} in the range -6 to -11 and $^{87}Sr/^{86}Sr_{182}$ >0.710 and therefore require an old lithospheric component in their source. Major element variations show that these intrusions were probably derived from a pyroxenite-rich source. A suite of basaltic-andesites and andesites exhibit major and trace element compositions that are similar to Ferrar dolerites, but they have εNd_{182} c. 0 and $^{87}Sr/^{86}Sr_{182}$ <0.7055 showing that they were derived from a less isotopically enriched source than the Ferrar dolerites. Basalt intrusions with $^{87}Sr/^{86}Sr_{182}$ c. 0.7035 and εNd_{182} c. +4, and low Th/Ta and La/Ta ratios (c. 1 and c. 15 respectively) escaped interaction with the lithosphere, and represent syn-break-up, asthenosphere-derived magmas emplaced at the initiation of oceanic spreading. Magmatism occurred on the periphery of the plume system centred on Dronning Maud Land, but there is no evidence to suggest that mantle potential temperatures were more than 1450°C in the Falkland Islands, leading to the possibility that melting occurred by decompression of mantle that had undergone internal heating whilst isolated beneath Gondwana for 100s of Ma.

The Early Jurassic (c. 180 Ma) Karoo and Ferrar large igneous provinces (LIP) were associated with Gondwana break-up. Two distinct geochemical associations of low TiO_2 continental flood basalts (CFB) have been identified on the basis of both their geochemical characteristics and geographical distribution. Igneous rocks of the Karoo province occur predominantly in South Africa but extend into Dronning Maud Land (Antarctica) with the main phase of activity taking place in the interval 178-184 Ma (Jourdan *et al.* 2004; 2005; 2007a; Riley *et al.* 2004). The Ferrar Province, which is contemporaneous with the magmatism in the Karoo province (Encarnacion *et al.* 1996; Fleming *et al*. 1997), is typified by the low TiO_2 Jurassic igneous rocks of the Transantarctic Mountains and Tasmania (Hergt *et al.* 1989; Fleming *et al.* 1995). It has also been established that the Karoo and Ferrar provinces have areas of geographical overlap, most notably in the KwaZulu area of South Africa (Riley *et al.* 2006; Sweeney *et al.* 1994) and in the Theron Mountains of Antarctica (Brewer *et al.* 1992). In the latter, at least four suites of low TiO_2 igneous rocks have been recognized, and it has been suggested that there is a transition from one province to the other rather, than a strict geographical delineation between the two provinces (Brewer *et al.* 1992). Hole (2015) argued that the melting to form the most magnesian Ferrar magmas required mantle potential temperatures (T_P) of c. 1450°C, around 100°C higher than ambient mantle (c. 1350±50°C) and consequently may have been generated by decompression melting of internally heated mantle melting being facilitated by Jurassic rifting. In this case there is no need for a mantle plume to generate Ferrar magmas. However, picritic magmatism in Dronning Maud Land, which was broadly synchronous with the emplacement of the Ferrar dolerites, required $T_P > 1550$°C, a temperature that is too high to be achieved by internal heating of the mantle and may therefore require the action of a hot mantle plume (Hole 2015; Coltice *et al.* 2009).

Elliott & Fleming (2000) argued that the focus of magmatism for both the Karoo and Ferrar provinces was the Weddell Triple Junction (WTJ; Fig. 1) which was within the envelope of a plume-related thermal anomaly associated with Gondwana break-up. Prior to Gondwana

fragmentation, plate reconstructions place the Falkland Islands on the extension of the Cape Fold Belt of South Africa, on the eastern flank of the Lebombo Rift (Fig. 1; Macdonald *et al.* 2003; Stone *et al.* 2008; 2009; Richards *et al.* 2013). By about 180 Ma, the islands had undergone 90° of rotation and consequently had passed over the locus of the WTJ. By the early Cretaceous (c. 135 Ma), the Falkland Islands had rotated a further 90° and had migrated to the west along the extension of the Aghulas Fracture zone to a position well to the west of the WTJ.

Since the Falkland Islands may have been very close to the focus of break-up related magmatism, it is logical to assume that the geochemical composition of any igneous rocks found in the islands should reflect the diversity of magmatism in the Jurassic Gondwana LIP as a whole. In this paper, new data are presented that show that the dykes and minor intrusions of the Falkland Islands exhibit variability in mineralogy, major element, trace element and Sr-, Nd- and Pb-isotopic compositions that is nearly as large as that seen in the entire Jurassic Gondwana LIP, even though the Falkland Islands themselves represent an area of 400km^2 kilometres. Intrusions with major and trace element characteristics most similar the Ferrar dolerites of the Transantarctic Mountain are juxtaposed with intrusions which are nearly identical to some Karoo basalts of South Africa and Antarctica.

Falkland Islands Dyke Swarm

Dolerite dykes, mostly of Jurassic age, are widespread in West Falkland and rather sparse in East Falkland (Fig. 2; Greenway 1972; Mussett & Taylor 1994; Thistlewood *et al.* 1997; Mitchell *et al.* 1999; Stone *et al.* 2008, 2009; Richards *et al.* 2013). Distinct sub-swarms of dykes have been recognized based on azimuth of exposed intrusions and aeromagnetic anomalies (Mitchell *et al.* 1999; Stone *et al.* 2009). Prominent dolerite dykes, tens of metres wide and oriented NE-SW, are present in both West and East Falkland and are reversely magnetized. This suite corresponds to the N-S suite of Mitchell *et al.* (1999), and is of Jurassic age (c. 178-188 Ma; Mussett & Taylor 1994; Stone *et al.* 2009). E-W oriented olivine-dolerite

74 dykes occur locally in the south of West Falkland, and they form part of a larger suite of
75 intrusions that Stone *et al.* (2009) suggest has a partially radial disposition. In addition, Richards
76 *et al.* (2013) noted that there is a suite of about 40, N-S oriented magnetic anomalies, that may
77 represent intrusions, and these occur across the entire Falkland Islands. Exposed examples from
78 Teal Creek and Peat Banks (Fig. 2) yield $^{40}Ar/^{39}Ar$ ages in the range 133-138 Ma and these
79 dykes are likely to be members of the Etendeka suite of south-western Africa (Stone *et al.* 2009;
80 Richards *et al.* 2013). During the current study, $^{40}Ar/^{39}Ar$ step-heating analysis was carried-out
81 on separated plagioclase feldspar phenocrysts from three samples, but only one of these yielded
82 useful information. Sample WI-5, a NE-SW oriented dyke from Weddell Island (Fig. 2), which
83 is also within the area of the radial swarm identified by Richards *et al.* (2013), contains
84 abundant plagioclase phenocrysts, and yielded a precise age of 182.3±1.5 Ma (Fig. 3). This
85 confirms a Jurassic age for some of the Falkland Islands intrusions, and it is within error of the
86 178.6±4.9 Ma determined by Stone *et al.* (2008) for an aphyric NE-SW dyke from Port Sussex
87 Creek, East Falkland (Fig. 2).

88 Selected major and trace element abundances *versus* weight % MgO for 139 intrusions from
89 the Falkland Islands, including 109 from this study and 30 from Mitchell *et al.* (1999), are
90 shown in Fig. 4 and representative analyses are given in Table 1. Mitchell *et al.* (1999) divided
91 the intrusions of the Falkland Islands into two main N-S and E-W suites based on azimuth, field
92 occurrence, petrography, mineral chemistry and whole-rock geochemical data. A subsidiary
93 three magma types were also tentatively identified by Mitchell *et al.* (1999), including 'evolved
94 N-S', Lively Island and Mount Alice types. The reassessment of the spatial distribution,
95 orientation and age of the dyke swarms by Stone *et al.* (2009) and Richards *et al.* (2013), along
96 with the much enlarged data set for the igneous rocks of the Falkland Islands generated for this
97 study, now allows the identification of six individual geochemical types of intrusions. The
98 criteria used to separate the different groups of intrusions are given in Table 2 and are illustrated
99 in Figs 4 to 10. A description of each suite is given below.

100 ***Port Sussex Creek-type intrusions (PST).*** All the N-S dykes of Mitchell *et al.* (1999) are
101 included in this suite of intrusions. PST intrusions are widely distributed across both East
102 Falkland and West Falkland, all are sub-vertical with an azimuth of NE-SW, and they are
103 consistently between 8 and 10 m in thickness. A typical example occurs at Port Sussex Creek,
104 East Falkland, (MHF1; Table 1, Fig. 2), and is an 8m wide, sub-vertical, medium-grained,
105 spheroidally-weathering dolerite dyke with an azimuth of 40º magnetic (NE-SW) and an age of
106 178.6±4.9Ma (Stone *et al.* 2008). The texture is equigranular and intersertal. Pyroxene is
107 enstatite ($En_{70}Wo_4Fs_{26}$), pigeonite ($En_{51}Wo_{13}Fs_{36}$) and augite (Fig. 7) and the feldspar is
108 labradorite (An_{70}). All PST intrusions contain both augite and pigeonite, with more mafic
109 samples containing orthopyroxene. Olivine (Fo_{50-71}) is rare in this suite of rocks and is restricted
110 to intrusions with Mg# >58 (e.g. FAR1503 and NGF16; Table 1, Fig. 4). Whole-rock MgO
111 contents vary from 5.9-9.5 weight % (Mg# 50-62) and SiO_2 (53-55 weight %) is higher for a
112 given MgO concentration than any of the other Falkland Islands intrusions (Fig. 4). The PST
113 intrusions are characterized by low CaO (8.1-9.8 weight %) for a given MgO content compared
114 to other Falkland Islands intrusions. TiO_2 abundances (0.9-1.2 weight %) are typical of the low
115 TiO_2 Gondwana break-up related LIPs of the southern hemisphere (Fig. 6). Abundances of Cr
116 are unusually high (up to 648 ppm) for samples with SiO_2 in their range, and are reflected in the
117 high Cr content of orthopyroxene. Abundances of Nb and Y are restricted to 2-5 and 19-23 ppm
118 respectively. PST intrusions are LREE enriched (Fig. 7) with $[La/Yb]_N$ in the range 3.2-3.9 and
119 samples lack any significant Eu anomaly (Eu/Eu* 0.89-0.97). La/Ta and Th/Ta are the highest
120 of any of the Falkland Islands samples analysed (44-52 and 5.9-8.6 respectively), and
121 consequently, on ORB-normalized multi-element diagrams (Fig. 8), samples exhibit a marked
122 trough in the abundances of Ta and Nb relative to Th, U, K and La (Fig. 9). $[Ta/Yb]_N$ is in the
123 range 2.0 to 2.6, the lowest values for any of the Falkland Islands intrusions. Ti/Zr and P/Zr (55-
124 60 and 4.5-6.3 respectively) are such that all PST intrusions exhibit a minor trough at Ti and P
125 relative to adjacent elements on ORB-normalized diagrams. εNd_{180} varies from -5.5 to -11.0 and

126 is accompanied by radiogenic Sr-isotopic compositions ($^{87}Sr/^{86}Sr_{180}$ 0.7070-0.7134), although
127 Sr-Nd isotope covariations are rather scattered (Fig. 9). Pb-isotopic compositions form an array
128 that is close to the Geochron ($^{207}Pb/^{204}Pb$ =15.55-15.65), and extends to $^{206}Pb/^{204}Pb$ ratios of up
129 to 18.40. $^{207}Pb/^{204}Pb$ exhibits a negative correlation with εNd_{180} for PST intrusions (Fig. 9).
130 Marked negative correlations between 1/Sr and $^{87}Sr/^{86}Sr_{182}$, εNd_{182} and Th/Ta and a positive
131 correlation between MgO and εNd_{182} suggests that PST dykes underwent interaction with a high
132 $^{87}Sr/^{86}Sr_{182}$ (> 0.714), low εNd_{182} (< -12) component that had Th/Ta > 9, and that interaction was
133 concomitant with crystallization (Fig. 10).
134 ***E-W intrusions.*** A description of this type of intrusions is given by Mitchell *et al.* (1999). E-W
135 intrusions are restricted to the central part of West Falkland (Fig. 2) and are generally medium-
136 grained olivine-phyric dolerites (Fo_{82} at 11 weight % MgO in the whole-rock), the only
137 pyroxene present being augite (Fig. 5). E-W intrusions are distinguished from the PST (Fig. 6)
138 by their lower SiO_2 contents (48-52 weight %) and higher Ti/Zr (80-95) for a similar range in
139 TiO_2, and MgO content (1.0-1.4 and 4.8-11.4 weight % respectively). E-W intrusions have
140 $[La/Yb]_N$ in the range 2.1-4.0 (Fig. 7) and no appreciable Eu anomaly (Eu/Eu* 0.89-1.0).
141 $[Ta/Yb]_N$ ratios are in the range 2.8 to 4.7, and all samples exhibit a negative Nb, Ta trough
142 relative to the LILE (La/Ta, 16-27, Th/Ta 2.2-2.8) but this is not as pronounced as that for the
143 PST intrusions. E-W intrusions have isotopic compositions that are close to, or slightly depleted
144 relative to the Chondritic Uniform Reservoir (εNd_{180} = -0.4 to 3.0; $^{87}Sr/^{86}Sr_{180}$= 0.7036-0.7058)
145 and have Pb-isotopic compositions that lie just above the NHRL (Fig. 9)
146 ***Lively Island intrusion.*** A single 30m thick intrusion which is exposed on Lively Island has
147 noticeably lower TiO_2 for a given MgO content than any other of the Falklands Islands
148 intrusions (TiO_2 = 0.8 weight % at 6 weight % MgO) and the data falls close to the
149 compositional trend for low TiO_2 Ferrar dolerites from the Transantarctic Mountains (Fig. 6).
150 Characteristic mineralogical features are the presence of sparse, Mg-rich biotite and rare Ca-
151 poor groundmass pyroxene (Fig. 5). The intrusion has a LREE-enriched REE profile ($[La/Yb]_N$

= 3.2) which lacks a significant negative Eu anomaly (Eu/Eu* = 0.87). La/Ta and Th/Ta (20.4 and 3.2 respectively) are similar to E-W intrusions and considerably lower than for PST intrusions (Table 2). The Lively Island intrusion contains radiogenic Nd and unradiogenic Sr (εNd_{180} -0.5, $^{87}Sr/^{86}Sr_{180}$ c. 0.7060) compared to PST intrusions.

Dyke Island Type (DIT). The greatest concentration of DIT intrusions is on aptly-named Dyke Island (Fig. 2). In addition, the evolved N-S samples described by Mitchell *et al.* (1999) are of this type (e.g. NHF17; Fig. 2). Intrusions are generally <50 cm thick, they may contain abundant plagioclase ± augite phenocrysts (samples WI-5, MHF14.9 and FAR338), or more commonly they are medium- to fined-grained aphyric basaltic-andesites and andesites with rare rhyolite sheets occurring locally. DIT intrusions represent an expanded fractionation series with MgO varying from 5.6 to <0.1 weight %, over a range of 51-75 weight % SiO_2. Ti/Zr is in the range 32-55 for samples with 4.0-5.6 weight % MgO, and for samples with <1 weight % MgO, Ti/Zr falls to <5 (Fig. 6). All DIT intrusions have higher concentrations of the incompatible elements Zr, Nb and Y than any of the other intrusions from the Falkland Islands, and exhibit strong positive linear correlations between these elements. On a plot of TiO_2 *versus* MgO (Fig. 6) DIT intrusions can be divided into three distinct series; i) a low TiO_2 series which forms and extension of the data array for PST intrusions; ii) a high TiO_2 series with MgO in the range 2.5-4.0 weight % MgO with TiO_2 > 1.7 weight %; and iii) acid intrusions with < 2 weight % MgO.

DIT intrusions are LREE-enriched ($[La/Yb]_N$ = 4.1-6.6; Fig. 7) and exhibit stepwise increases in both LREE and HREE abundances with decreasing MgO with the most evolved sample (MHF41.3, 0.06 weight % MgO) having La_N = 290 and Yb_N = 44. The development of a progressively larger negative Eu anomaly (Eu/Eu* 0.85-0.71) with decreasing MgO, attests to the importance of plagioclase fractionation during their petrogenesis. Th/Ta and La/Ta for the DIT intrusions (2.4-3.4 and 17-26 respectively) are similar to those for the E-W intrusions. Multi-element diagrams (Fig. 8) show that DIT intrusions exhibit troughs at Ti and P relative to

adjacent elements, and a progressively larger negative Sr anomaly is developed with decreasing MgO. Plagioclase-phyric samples WI-5 and FAR338 exhibit a positive Sr spike in Fig. 8, which is presumably a result of accumulation of plagioclase feldspar, although neither sample exhibits a Eu anomaly. The distribution of trace elements in DIT intrusions bears a strong resemblance to those for Ferrar dolerites from the Transantarctic Mountains (Fig. 8). DIT intrusions have $^{87}Sr/^{86}Sr_{180}$ in the range 0.7055-0.7170 but all samples with $^{87}Sr/^{86}Sr_{182} > 0.7090$ contain < 2 weight % MgO. εNd_{182} falls in the range -2.8 to +0.6, and there is no systematic variation between MgO, εNd_{182} or $^{87}Sr/^{86}Sr_{182}$ (Figs 9 & 10).

Mount Alice Type intrusions (MAT). MAT intrusions are restricted to the south-western area of West Falkland, around South Harbour, Dyke Island and Cape Orford (Fig.1) and are early Jurassic in age (188±2 Ma for sample MA3; Mussett & Taylor 1994). MAT intrusions are generally < 1 m thick and are characterized by plagioclase ± augite ± olivine phenocrysts in a fine-grained groundmass. Since the area in which the MAT intrusions occur is within the region of the radial dyke swarm described Richards *et al.* (2013), azimuths cannot be used as one of their classification criteria, although in the region of Cape Orford, MAT dykes are generally oriented E-W (Mussett & Taylor 1994; Thistlewood *et al.* 1997). A typical example (MFH15.2) contains sparse, scattered phenocrysts of olivine (Fo_{80}), calcic augite ($En_{31}Fs_{25}Wo_{44}$; Fig. 5) and labradorite (An_{60}). MgO varies from 6-12 weight %, and the MAT intrusions have the lowest SiO_2 (46-50 weight %) for a given MgO content of any of the Falklands Islands samples (Fig. 4). TiO_2 abundances (1.3-2.0 weight %) overlap with those for both the PST and E-W intrusions but Ti/Zr is in the range 90-150 which is considerably higher than any other of the Falkland Islands intrusions. MAT intrusions have $[La/Yb]_N$ in the range 1.8-3.1 (Fig. 7) and flat to slightly LREE-depleted REE profiles for elements La to Sm ($[La/Sm]_N$ 0.9-1.5). On multi-element diagrams (Fig. 8), MAT intrusions exhibit a positive Sr spike relative to N-ORB, but otherwise have smooth profiles from elements Nd to Lu, with Ti/Zr and P/Zr (98-130 and 8.0-10.4 respectively) in the range for normal ORB (Ti/Zr c. 100, P/Zr c. 6.9; Sun & McDonough

1987). Unlike all the other Falkland Islands intrusions, the MAT have Th/Ta and La/Ta (0.7-1.0 and 13-17 respectively) which are also within the range for normal ocean ridge basalts and asthenosphere-derived basalts (Sun & McDonough 1987). Sr- & Nd-isotopic compositions fall in the upper-left quadrant of Fig. 10, with $\varepsilon Nd_{180} > 5$ and $^{87}Sr/^{86}Sr_{180} < 0.7040$. Pb-isotopic compositions fall just above the NHRL with $^{206}Pb/^{204}Pb$ in the range 18.2-18.5 (Fig. 9).

Provinciality of Falkland Islands intrusions

The Karoo and Ferrar LIPs can be separated from one another on the basis of MgO, SiO_2, TiO_2 content and Ti/Zr. These differences are illustrated in Fig. 6. The Ferrar LIP has two distinct lineages of igneous rocks one of which is typified by the low TiO_2 and low Ti/Zr basalts and basaltic-andesites of the Transantarctic Mountains and the other by the slightly higher TiO_2 series of the Theron Mountains (Fig. 5). Brewer *et al*. (1992) argued that the Theron Mountinas represented the geographical region of overlap of the Karoo and Ferrar LIPs. Ferrar LIP volcanic rocks have also been recognized in southern Africa (Riley *et al*. 2006) and so the geographical distribution of Ferrar LIP igneous rocks is not simple. Karoo LIP igneous rocks belong to a higher TiO_2 and lower SiO_2 suite than the Ferrar LIP. Within Dronning Maud Land, at least four component magma types of the Karoo LIP have been recognized (Fig. 5). These comprise chemical types CT1, CT2 and CT3 (Luttinen *et al.* 1998; Luttinen & Furnes (2000), plus the dolerites of the Kirwanveggan (Harris *et al.* 1990). There is a total overlap in the MgO, SiO_2, TiO_2 content and Ti/Zr of the Dronning Maud Land igneous rocks and those of South Africa (not shown).

Figure 6 shows that PST intrusions exhibit similar variations in MgO, TiO_2 and Ti/Zr to the low TiO_2 suite of the Theron Mountains (Brewer *et al.* 1992) and to CT1 basalts of Dronning Maud Land (Luttinen & Furnes 2000). However, the limited SiO_2 content of the PST intrusions suggests a stronger affinity with CT1 basalts than Theron Mountains samples, the latter of which have a much broader range in SiO_2 than CT1 and PST samples. Whilst E-W intrusions

have ranges in MgO, SiO_2 and TiO_2 contents that are typical of Karoo LIP igneous rock, Ti/Zr ~80 and SiO_2 47-52 weight % are closest to the composition of basalts from Kirwanveggan and Schirmacher Oasis, Dronning Maud Land (Fig. 8; Harris *et al.* 1990; Sushchevskaya *et al.* 2009). DIT intrusions exhibit similar distributions in MgO and TiO_2 to basalts and basaltic-andesites from the Theron Mountains (Brewer *et al.* 1992) and Transantarctic Mountains (Fleming *et al*. 1995). Evolved (SiO_2 > 60 weight %) igneous rocks, similar to some of the DIT intrusions, have also been reported from the Transantarctic Mountains and Tasmania (Melluso *et al*. 2013). Characteristic features of intermediate compositions from the Transantarctic Mountains are troughs at Sr, Ti and P on multi-element diagrams (Fig. 8) which DIT samples with < 5 weight % MgO share. MAT intrusions have unusually high Ti/Zr (85-150) a characteristic that they share with CT2 and CT3 basalts of Dronning Maud Land and Rooi Rand ORB-like dykes (Melluso *et al*. 2008) from the Southern Lebombo of Africa (Fig. 6). Given that the data shown in Fig. 5 encompasses the entire compositional variability within the Karoo and Ferrar LIPs, it is striking that the majority of the low TiO_2 break-up related magma types are all represented within a small geographical area of the Falkland Islands. Indeed, within an area of 400km^2 centred on Dyke Island, magma types representing compositions similar to the CT1 and Kirwanveggan of Dronning Maud Land, the low and high TiO_2 dolerites of the Theron Mountains, and intermediate to acid compositions of the Transantarctic Mountains and Tasmania are all represented. The geographical boundaries of the Karoo and Ferrar LIPs therefore requires re-evaluation. Firstly the detailed petrogenetic history of the different groups of Falkand Islands intrusions will be considered.

Petrogenesis of the Falkland Islands intrusions

PST intrusions

PST and low TiO_2 DIT intrusions exhibit variations in major element compositions that fall along the same fractionation trend as low TiO_2 basaltic-andesites and andesites from the Theron Mountains (Figs. 5 & 6). However, PST and DIT intrusions cannot be related to one another by

254 simple crystal fractionation because their Sr-, Nd- and Pb-isotopic compositions differ
255 significantly from one another (Fig. 10). The high $^{87}Sr/^{86}Sr_{182}$ (> 0.710) and unradiogenic Nd-
256 isotopic compositions of the PST is a feature they share with Ferrar dolerites. Fleming *et al.*
257 (1995) and Molzhan *et al.* (1999) demonstrated that the relatively consistent εNd_{182} (-4.8 to -
258 5.4), but highly variable $^{87}Sr/^{86}Sr_{182}$ (0.7090-0.7112) of the MFCT was partly a function of Rb
259 and Sr mobility during a Cretaceous (97-125 Ma) hydrothermal event. This cannot be used as
260 an explanation for variability in the Sr-isotopic compositions of PST intrusions because the
261 Falkland Islands would have already broken-away from the Antarctic continent by this time. In
262 addition, the range of εNd_{182} from -6 to -12 over the limited range of $^{87}Sr/^{86}Sr_{182}$ = 0.7110-
263 0.7115, requires potential contaminants that had a range of Nd-isotopic compositions and were
264 therefore probably of differing ages.
265 **Interaction with the continental lithosphere.** For the PST intrusions, the variations shown in
266 Fig. 10 indicate that Sr- and Nd-isotopic variations were imposed on the magmas concomitant
267 with fractional crystallization, by assimilation with fractional crystallization (AFC) or a similar
268 process. The relationships shown in Fig. 10 require that Sr behaved incompatibly during
269 fractional crystallization of the PST suite. The crystal cumulate formed during AFC cannot,
270 therefore, have been plagioclase-rich. Least-squares modelling of the extract and evolved liquid
271 from a starting composition with 9.6 weight % MgO (NGF16) to evolved composition with 6.78
272 weight % MgO (MHF5.1; Table 3) requires 21% crystallization of an assemblage of
273 orthopyroxene (74.7%), plagioclase (18.9%) and minor augite (6.4%). With only 18.9% of the
274 fractionating assemblage being plagioclase, DSr would have been <1 which is consistent with
275 the relationship between 1/Sr and $^{87}Sr/^{86}Sr_{182}$ in Fig. 10. Consequently, to generate the range of
276 Sr-isotopic compositions seen in the PST intrusions requires a source with $^{87}Sr/^{86}Sr_{182} \leq 0.7075$,
277 and contaminants with $^{87}Sr/^{86}Sr_{182} > 0.7130$ and a range of εNd_{182}, which must be ≤ -6.0 for all
278 samples.

279 Sr- and Nd-isotopic compositions for PST intrusions fall in an intermediate position between
280 the data for CT1 basalts of Dronning Maud Land and the Karoo (Fig. 11). Luttinen & Furnes
281 (2000) argued that the extreme Nd-isotopic compositions ($\varepsilon Nd_{182} \leq -17$) of CT1 basalts were the
282 result of interaction between a mantle-derived magma and Archean (3.0 Ga) Grunehogna
283 cratonic lithosphere (Fig. 1). Riley *et al.* (2006) used AFC and energy-constrained recharge
284 AFC to model the isotopic compositions of Karoo basalts using an ORB-like source and an
285 assimilant with $\varepsilon Nd_{182} = -4$ and $^{87}Sr/^{86}Sr_{182} = 0.710$, and showed that the observed isotopic
286 variability in the basalts could be explained partly by these processes. In Fig. 11 three AFC
287 trajectories are plotted and the parameters used to generate the curves are given in Table 4.
288 These are not designed to fully explain the isotopic diversity in Gondwana low TiO_2 CFB, they
289 have been generated in an attempt to constrain possible and impossible petrogenetic processes.
290 The starting composition has been kept constant, and is based on that that of largely
291 uncontaminated low TiO_2 basalts with $\varepsilon Nd_{182} = 2$ and $^{87}Sr/^{86}Sr_{182} = 0.7035$. For all three
292 modelled AFC trends, the ratio of the country rock assimilated to crystal cumulate formed, *R*,
293 has be set at 0.40, a value that is appropriate for crystallization in the middle- to upper-crust
294 (Riley *et al.* 2006; Hole *et al*. 2015). D_{Sr} and D_{Nd} are set at 0.5 and 0.1 respectively, to simulate a
295 cumulate with approximately 25% plagioclase, and 75% ferromagnesian minerals. This means
296 that all three AFC trajectories approach the composition of the most contaminated magma for ≤
297 20% AFC (Table 4). Increasing the value of *R* to 0.5 for any of the models does not significantly
298 change the shape of the trajectories, but decreases the amount of AFC that is needed to reach the
299 target compositions to ≤12%., and conversely, decreasing R to 0.3 requires ≤ 25% AFC. For the
300 CT1 AFC model, the contaminant represents 3.0 Ga Grunehogen Craton (Fig. 1) felsic granulite,
301 with $\varepsilon Nd_{182} = -50$ and $^{87}Sr/^{86}Sr_{182} = 0.712$ (felsic xenolith sample X4-AVL of Luttinen & Furnes
302 2000). The PST-1, mixing line intersects the lowest εNd_{182} samples in the PST suite, and the
303 contaminant represents a 2.2 Ga Palaeoproterzoic felsic granulite with $\varepsilon Nd_{182} = -20$ and
304 $^{87}Sr/^{86}Sr_{182} = 0.720$. The PST-2 mixing line, which also intersects the majority of data for Karoo

basalts and lowest $^{87}Sr/^{86}Sr_{180}$ (~0.7090) Ferrar dolerites, representing mixing between a mantle-derived magma and 1.0-1.5 Ga felsic crust with εNd_{182} = -10. Plate reconstructions place the Falkland Islands mainly within the 1.0-1.5 Ga Namaqualand-Natal-Maudheim-Mozambique belt (Thistlewood *et al.* 1997) and on the continuation of the Cape Fold Belt (Fig. 1). Mesoproterozoic crust is therefore a likely candidate for basement to the Falkland Islands. What is also clear is that cratonic basement like that involved in the petrogensis of the CT1 basalts affects neither the PST intrusions nor Karoo low TiO_2 basalts. AFC models with geologically reasonable parameters and appropriate ages of potential basement contaminants can therefore produce the observed variations in the Sr- and Nd-isotopic characteristics of the PST intrusions for < 20% AFC.

Pyroxenite *versus* peridotite sources. PST intrusions with MgO > 8 weight % have lower CaO abundances (c. 8.5 weight %) than any other of the other Falkland Islands intrusions (Figs. 4 and 12). Such compositions are uncommon in continental flood basalts provinces. Orthopyroxene was the dominant fractionating phase during crystallization of the PST (Table 3) and estimates of more primitive compositions can be calculated by incrementally adding enstatite to a mafic PST composition. Addition of 30% enstatite to sample NGF16 yields magma with ~15 weight % MgO and ~7.5 weight % CaO. Compositions such as these are also found in the CT1 basalts of Dronning Maud Land (Figs 12 and 13). An unusual feature of the PST intrusions is their Si-oversaturated nature and high Cr content (Fig. 12) which is also reflected in unusually high Cr content of component orthopyroxene (e.g. enstatite in MHF3.2 has 0.74 weight % Cr_2O_3 at MgO/FeO = 2.8). In terms of major element compositions, PST intrusions bear strong similarities with magnesian andesite from continental subduction settings (e.g. Baker *et al.* 1994; Sato *et al.* 2014). For example, high-Mg andesites from Mt Shasta have a similar range of MgO to PST intrusions (Fig. 12) which is accompanied by SiO_2 = 51.5-54.0 weight %, Cr = 245-695 ppm, Ni =99-235 ppm, TiO_2 = 0.6-0.8 weight % and CaO =8.6-9.6 weight %. One

330 mechanism that has been suggested for the production of high-Mg andesite is the interaction of
331 slab-derived adakitic melts with mantle peridotite during subduction (Heinonen *et al.* 2014). A
332 link to the previous subduction history of the mantle source from which Ferrar and Karoo
333 basalts were derived has been made by a number of workers (e.g. Brewer *et al.* 1992; Storey *et*
334 *al.* 1992; Heinonen *et al.* 2014) and in particular, the characteristic trough at Nb and Ta relative
335 to adjacent elements (Fig. 9) has been interpreted as an inherited subduction signature.
336 Herzberg & Asimow (2008) note that primary magmas derived from the melting of
337 pyroxenite will exhibit relative CaO depletion compared to melts from a peridotite source
338 because of the dominance of residual clinopyroxene in the source region during partial melting
339 of pyroxenite. Given the position that data for the PST occupy in Fig. 12, it seems clear that
340 their major element compositions are not consistent with an origin by melting of mantle
341 peridotite. It is well established that pyroxenite can be formed at the base of the lithosphere as a
342 result of accumulation of mafic phases during basaltic magmatism (e.g. Downes *et al.* 2007).
343 Such accumulative pyroxenite can yield magma by partial melting at some later stage, promoted
344 by a new phase of mafic magmatism and by interaction with peridotite-derived melts (Lambart
345 *et al.* 2013). The generation of silica-enriched pyroxenite melts is possible, which can yield Si-
346 oversaturated melts like those of the PST intrusions (Lambart *et al.* 2013). It is therefore
347 suggested that the PST were derived from a pyroxenite-rich source that was emplaced at the
348 base of the lithosphere during the prolonged subduction history of Gondwana. Metasomatism of
349 the pyroxenite by slab-derived fluids and melt, imparted a subduction signature to the
350 pyroxenite. When subjected to the high mantle potential temperatures associated with the mantle
351 plume beneath Dronning Maud Land at c. 180 Ma (T_P up to 1600°C; Heinonen *et al.* 2010), the
352 pyroxenite underwent partial melting and produced the primary melt precursor to the PST
353 intrusions. These melts then interacted with fusible, felsic continental crust to produce the
354 geochemical composition of the more evolved PST compositions by AFC, or a related process.
355 Extrapolation of the MgO - εNd_{180} trend for the PST to higher MgO contents (Fig. 10), suggests

356 that a primitive composition with 15 weight % MgO might have had εNd_{180} ~0, and the
357 correlation between 1/Sr and Sr-isotopic compositions requires the source to have $^{87}Sr/^{86}Sr_{182} \leq$
358 0.7075.

359 ***DIT and Lively Island intrusions***

360 In contrast to the PST intrusions, the sub-horizontal arrays delineated by DIT intrusions in Fig.
361 10a, suggests that AFC or a similar process was not important during their petrogenesis.
362 However, a negative correlation between Th/Ta and εNd_{182} for the DIT intrusions (Fig. 10b)
363 may require minor modification by a crustal component with Th/Ta $\geq$ 3.0. A characteristic
364 feature of the DIT samples is that they have εNd_{182} in range -2.8 to +0.6, but with only a single
365 analysed sample (NHF17) having $\varepsilon Nd_{182} < -1$. In addition, the Lively Island dyke, which falls
366 close to the fractionation trend for the MFCT dolerites of the Transantarctic Mountains (Fig. 6),
367 has Sr- and Nd-isotopic compositions ($^{87}Sr/^{86}Sr_{182}$ c. 0.7052, εNd_{182} = -0.5 to -1.4) that do not
368 require the significant isotopic enrichment seen in the Ferrar dolerites (εNd_{182} in the range -3.3
369 to -5.3; Fleming *et al.* 1995). The source of the low TiO_2 DIT magmas could, therefore, have
370 had $\varepsilon Nd_{182} > 0$, $^{87}Sr/^{86}Sr_{182} < 0.7050$, Th/Ta < 2.5 and La/Ta < 20. Nevertheless, there are
371 striking similarities between the major trace element composition of the DIT and Lively Island
372 intrusions and those of Ferrar dolerites of the Transantarctic and Theron mountains and the
373 dolerites of Tasmania (e.g. Figs 6 and 13).

374 It has been argued that depleted mantle-like Os-isotopic signatures of Ferrar and Tasmanian
375 dolerites, along with $\delta^{18}O$ of 5 to 7‰, are not consistent with an AFC process involving upper-
376 or lower-crust, but are more likely to reflect source contamination involving interaction between
377 mantle peridotite and recycled upper-crustal materials (Molzhan *et al.* 1996; Brauns *et al.* 2000).
378 γ_{Os} values of -10 to +10 for harzburgite and lherzolite xenoliths from the sub-continental
379 lithospheric mantle beneath SE Australia overlap with the range of γ_{Os} for the Tasmanian and
380 Ferrar dolerites (γ_{Os} = -2 ± 25; these relatively large ranges in γ_{Os} reflect uncertainties in the

estimates of initial $^{187}Os/^{188}Os$ ratios, rather than being a measured range of values). In addition, basalts and picrites from Dronning Maud Land have εNd_{182} = +8.0 to -2.2 and γ_{Os} in the range -1 to +10 reflecting a similar origin (Heinonen *et al.* 2010). It must be argued, therefore, that the unradiogenic Nd-isotopic compositions of the Ferrar dolerites must result from an ancient enrichment in Nd relative to Sm in their source, which may also have been accompanied by enrichment of the LILE relative to HFSE. It is therefore suggested that the DIT magmas were derived from a similar mantle source region to that of the Ferrar dolerites, but one which had experienced significantly less LILE and LREE enrichment to that that seen in the Transantarctic Mountains. Basalts from the Theron Mountains have εNd_{182} = -1.3 to -5.7, values which are transitional between those of the DIT intrusions and Ferrar dolerites (Brewer *et al.* 1992). There is, therefore, a geographical variability in LILE/HFSE and εNd_{182} is within the Jurassic low TiO_2 basalts of West Antarctica.

MAT intrusions

The positive εNd_{182} (2.7-3.6) and low Th/Ta, La/Ta and $[La/Yb]_N$ (0.8-1.0; 12.8-17.3 and 1.9-3.7 respectively) of MAT intrusions suggests that they were derived from an asthenospheric source, and escaped significant interaction with lithosphere. Such compositions are also known from the Southern Lebombo Rift and within Dronning Maud Land (Fig. 8). The most satisfactory explanation for the geochemical compositions of these rocks is that they were generated by decompression melting of the asthenosphere during the rifting stage of Gondwana break-up. In this respect they have similar geochemical compositions to the ORB-like Rooi Rand basaltic dykes of the southern Lebombo, which post-date the main magmatic phases in the region by about 5 Myr (Jourdan *et al.* 2007b).

Cretaceous intrusions

Until more data are forthcoming, the origin and affinity of the Cretaceous Teal Creek intrusion reported by Stone *et al.* (2009) remains somewhat obscure. Major element data for the intrusion

406 plot close to the Theron Mountains low TiO_2 trend in Fig. 5, but the intrusion has higher Fe_2O_3
407 (c. 15.9 weight %) at 5.7 weight % MgO than any of the data for the intrusions presented here.
408 What is clear, is that there is an extensive suite of low TiO_2 basalts within the Etendeka
409 Province (e.g. Gibson *et al.* 2005; Thompson *et al.* 2001) from which it could be sourced.
410 However, none of the groups of intrusions described here carries a similar signature to that
411 presented by Stone *et al.* (2009) for the Teal Creak dyke.

412 ## Mantle potential temperature, rifting and magmatism

413 Fig. 14a summarizes the available data for olivine equilibration temperatures (T_{OL}) for MAT
414 and E-W basalts and picrites from Dronning Maud. MAT and E-W basalts yield olivine
415 equilibration temperatures of 1245°C and 1330°C respectively, using the method of Putirka *et*
416 *al.* (2007), whilst olivine in picrites from Dronning Maud Land yield T_{OL} up to 1450°C.
417 Converting equilibration temperatures to T_P is problematical if the pressure and extent of
418 melting cannot be independently determined (Herzburg & Asomow 2008; Herzburg & Gazel
419 2009; Hole 2015), which they cannot for the MAT and E-W samples. However, since olivine
420 equilibration temperature increases with increasing pressure of crystallization, synthetic olivine
421 liquidi can be calculated for any given temperature and pressure (Herzberg & Gazel 2009). Fig.
422 13b shows the inferred temperature-pressure conditions at which fractional melting terminated
423 for calculated primary magmas from Dronning Maud Land, the Karoo Province of southern
424 Africa, Ferrar dolerites of Antarctica calculated following the methods of Herzberg & Gazel
425 (2009) and Hole (2015).

426 Also shown in Fig. 13 for are data for basalts from the Cretaceous Etendeka Province of SW
427 Africa (Kieding *et al.* 2011) for which estimates of T_{OL}, estimates of T_P from melt inclusions in
428 ultra-magnesian olivine, and estimates of T_P from the PRIMEL2 model of Herzberg & Asimow
429 (2008) have all been calculated on the same samples. Using the Herzberg & Asimow (2008)
430 model yields T_P = 1500-1550°C and final pressures of melting (P*f*) between 1.5 and 4.0 GPa
431 (Fig. 13a). T_P from melt inclusions is 1300-1520°C, whilst T_{OL} is in the range 1250-1400°C and

there is an empirical relationship between T_{OL} and melt inclusion T_P which approximates to $T_P = 1.443\ T_{ol} - 501$ for the Etendeka plume system (Fig. 13c). Therefore is seems that within a single plume system, basalts may be generated over ranges of T_P that are larger than the ±50°C error inherent in the calculation methods (Herzberg & Asimow 2009; Hole 2015). Direct application of this empirical observation to the Dronning Maud Land picrites suggest maximum $T_P \sim 1550$°C, a temperature that is considered to be associated with 'hot' mantle plumes such as Iceland at 60 Ma (Fig. 13a; Herzberg & Gazel 2009). However, indications of $T_P \sim 1300$°C are also evident from the Dronning Maud Land data. For Falkland Islands E-W basalts, $T_{OL} \sim 1330$°C, which implies $T_P \sim 1400$°C and for olivine-phyric MAT basalts, $T_{OL} \sim 1250$°C implying $T_P \sim 1300$°C. These T_P estimates for the Falkland Islands E-W and MAT basalts may therefore be reconciled with a model involving melting of mantle with near-ambient temperature ($T_P \geq 1350$°C), but would require intersection of the dry peridotite solidus at ~2.1 GPa (~70km) and all melting to take place in the garnet stability field of the mantle; the most mafic MAT and E-W intrusions have $[La/Yb]_N < 2.0$ which does not preclude such an origin. Additionally, near-ambient T_P melting would require the continental lithosphere to be thinned substantially and perhaps to < 50km, to allow decompression melting to take place. Gondwana fragmentation could have provided the necessary extensional tectonism to allow for such lithospheric thinning. Whilst there is no primary evidence to suggest T_P was > 1450°C beneath the Falkland Islands at 180 Ma, it is possible that high-MgO large melt fractions requiring substantially higher T_P exist in the region, but they have not been sampled, remains a possibility.

The diversity of magma types found in the Falkland Islands, and the position of the islands in a 180 Ma plate reconstruction (Fig. 1) is entirely consistent with the their being close to the focus of magmatism during continental break-up. We concur with Brewer *et al*. (1992) and Riley *et al*. (2006) that there is considerable overlap in the geographical distribution of the Ferrar and Karoo LIPs, which is most obvious in the Theron Mountains. It is also clear, that despite the wealth of geochemical data available for the Transantarctic Mountains and

458 Tasmania, there is no evidence to suggest that volcanic rocks with affinities to the Karoo LIP
459 occur in those areas. The broadly linear distribution of Ferrar LIP volcanic rocks has been
460 attributed to syn- or pre-volcanic rifting (Elliot 2013) with lava flows fed from shallow (< 4 km
461 depth) sills intruding Early Jurassic Mawson Group and equivalent sedimentary rocks
462 (Muirhead *et al.* 2014). Pillow basalts and palagonite successions, at the base of the lava pile
463 along with the substantial thickness of many lava flows in the Transantarctic Mountains, suggest
464 confining topography and emplacement into a rift system (Elliot 2013). Stratigraphical
465 confinement of early magmatism to extensional basins is a feature of a number of LIPs (e.g.
466 North Atlantic Igneous Province, Williamson & Bell 2012; Hole *et al.* 2015; Central Atlantic
467 Magmatic Province; Coltice *et al.* 2009; Hole 2015). Emplacement of Ferrar magmas into an
468 active rift is therefore consistent with the magmatic plumbing (Muirhead *et al*. 2014), the style
469 of volcanic activity at the base of the system, and the linear distribution of volcanism. In
470 addition, Storey *et al.* (1988) also noted that Ferrar basaltic volcanism was synchronous with
471 within-plate granitic magmatism in the Ellsworth Mountains (Fig. 1), sodic-alkaline intrusions
472 being emplaced through dilated crust in rift-controlled loci. It has also been argued that some of
473 the most magnesian Ferrar dolerites were generated by decompression melting of internally
474 heated mantle in an active rift zone beneath which mantle potential temperature (T_P) was 1450 ±
475 50°C (Hole 2015). If this is the case, then the action of a hot mantle plume is not required for
476 Ferrar magmatism (Hole 2015) and may also not be required for magmatism in the Falkland
477 Islands which were situated on an extension of the Ferrar-Theron Mountains rift system at 180
478 Ma.

479 With the exception of the ORB-like basalts of the Rooi Rand dyke swarm (Marsh *et al.* 1997;
480 Mitchell *et al.* 1999) which represent syn-break-up magmas, Karoo magmatism does not appear
481 to be geographically restricted in the same manner as Ferrar magmatism, and basalts with
482 Karoo-type geochemical compositions only extend as far as the overlap zone in the Theron
483 Mountains. In addition, along the zone of the Ferrar LIP, continental break-up failed, whereas

484 the Karoo was close to the locus of the formation of three triple junctions (Fig. 1). It is therefore
485 suggested that Ferrar LIP magmatism was limited to the zone of extensional tectonism,
486 extension being driven by plate-boundary forces in a similar manner to that which controls part
487 of the NAIP (Nielsen *et al.* 2007; Hole *et al.* 2015). Within this rift, magmatism occurred
488 because of decompression melting of internally heated mantle. Conversely, the high mantle
489 potential temperatures (T_P up to 1550°C) required for the generation of some Dronning Maud
490 Land break-up related picrite magmas (Heinonen & Luttinen 2010) suggests proximity to a
491 plume head. It was this plume head that drove the break-up Antarctica and South Africa, but the
492 Falkland Islands would have been on its periphery, as would the Theron Mountains.

493 ## Conclusions

494 The Jurassic (c. 182 Ma) intrusions of the Falkland Islands exhibit a broad range of
495 geochemical compositions that encompass much of the variability seen in the Karoo and Ferrar
496 LIPs. PST intrusions were derived from by melting of a pyroxenite-rich source that had been
497 enriched in LILE during the prior subduction history of this part of Gondwana. Magmas
498 subsequently interacted with 'old' (c. 2.2 Ga) fusible continental lithospheric components by a
499 AFC or a related process. DIT intrusions have trace element signatures that are very similar to
500 volcanic rocks of the Ferrar LIP, but some samples have noticeably unradiogenic Sr- and
501 radiogenic Nd-isotopic compositions ($^{87}Sr/^{86}Sr_{182} \sim 0.7050$ and $\varepsilon Nd_{182} \sim 0$) compared to most
502 other Ferrar LIP igneous rocks. This suggests that the source of the Ferrar dolerites is not
503 necessarily particularly isotopically enriched. Basalts with radiogenic Nd- and unradiogenic Sr-
504 isotopic compositions ($^{87}Sr/^{86}Sr_{182} < 0.7045$ and εNd_{182} +4) also have Th/Ta and La/Ta (~1.0
505 and 17 respectively) that require little input from the continental lithosphere. These basalts were
506 probably emplaced syn-break-up and are likened to the Rooi Rand dykes of the Southern
507 Lebombo of Africa.

508 Early Jurassic plate reconstructions place the Falkland Islands close to the Weddell Triple
509 Junction, at the proximity of the islands to the area of overlap between Karoo and Ferrar LIPs

510 explains the diversity of igneous rock compositions. Whilst Ferrar and Karoo LIP igneous rocks
511 show overlapping distributions in the Theron Mountains Falkland Islands and southern Africa,
512 there is no evidence for Karoo-type magmas within the majority of the Ferrar LIP. In addition,
513 whilst there are basalts within the Karoo LIP that require $T_P \geq 1550°C$, the Ferrar LIP, and
514 equivalent magma types in the Falkland Islands (i.e. DIT intrusions) were unrelated to a mantle
515 plume and were formed by decompression melting of internally heated mantle with $T_P \leq 1450°C$.
516 The Ferrar LIP was emplaced into actively extending continental lithosphere, with extension
517 being driven by pre-break-up plate boundary forces. The Karoo province owes its existence to
518 a hot mantle plume that was centred near the boundary of what is now Dronning Maud Land and
519 the eastern part of South Africa. The diversity of the magmatism in the Falkland Islands has its
520 origins in the fact that the islands occupied a position towards the extremity of both the rift
521 system and the extremity of the plume system centred on Dronning Maud Land.
522

References Cited.

Antonini, P., Piccirillo, E.M., Petrini, R., Civetta, M., D'Antonio, M. & Orsi, G. 1999. Enriched mantle Dupal signature in the genesis of the Jurassic Ferrar tholeiites from the Prince Albert Mountains, (Victoria Land, Antarctica). *Contributions to Mineralogy and Petrology*, **136**, 1-19.

Baker, M.B., Grove, T.L. and Price, R.C. 1994. Primitive basalts and andesites from the Mt. Shasta region, N. California: products of varying melt fraction and water content. *Contributions to Mineralogy and Petrology*, **118**, 111-129.

Baranov, A. & Morelli. A. 2013. The Moho depth map of Antarctica. *Tectonophysics*, **609**, 299-313.

Brauns, C.M., Hergt, J.M. Woodhead, J.D. & Maas, R. 2000. Os isotopes and the origin of the Tasmanian dolerites. *Journal of Petrology*, **41**, 905-918.

Brewer, T. S., Hergt, J. M., Hawkesworth, C. J., Rex D. C. & Storey B. C. 1992. Coats Land dolerites and the generation of Antarctic continental flood basalts. *In:* Storey, B. C., Alabaster, T. & Pankhurst, R. J. (eds) *Magmatism and the causes of Continental Break-Up* Geological Society, London, Special Publications, **64,** 185-208.

Coltice, N., Bertrand, H., Rey, P.M., Jourdan, F., Phillips, B.R. & Ricard, Y. 2009. Global warming of the mantle beneath continents back to the Archaean. *Gondwana Research*, **15**, 254-266.

Demarchi, G., Antonini, P., Piccirillo, E.M., Orsi, G., Civetta, L. & D'Antonini, M. 2001. Significance of orthopyroxene and major element constraints on the petrogenesis of Ferrar tholeiites from southern Prince Albert Mountains, Victoria Land, Antarctica. *Contributions to Mineralogy and Petrology*, **142**, 127-146.

Downes, H., Upton, B.G.J., Connolly, J., Beard, A.D. & Bodinier, J-L 2007. Evidence for late Palaeozoic crustal underplating beneath SW Scotland Petrology and geochemistry of a cumulate xenolith suite from Bute. *Journal of the Geological Society, London*, **164**, 1217-1231.

Elliot, D.H. 2013. The geological and tectonic evolution of the Transantarctic Mountains: a review. *In:* Hambrey, M.J., Barker, P.F., Barrett, P.J., Bowman, V., Davies, B., Smellie, J.L. & Tranter, M (eds). *Antarctic Palaeoenvironments and Earth-surface process*. Geological Society London, Special Publications, **381**, 7-35.

Elliot, D. H. & Fleming, T. H. 2000. Weddell Triple Junction: The principal focus of Ferrar and Karoo magmatism during the initial break-up of Gondwana. *Geology*, **28**, 539-542.

556 Elliot, D. H. & Fleming, T. H. 2004. Occurrence and Dispersal of Magmas in the Jurassic Ferrar
557 Large Igneous Province, Antarctica. *Gondwana Research*, B, 223-237.
558 Elliot, D.H., Fleming, T.H., Haban, M.A. & Siders, M.A. 1995. Petrology and mineralogy of the
559 Kirkpatrick Basalt and Ferrar Dolerite, Mesa Region, Northern Vitoria Land, Antarctica. *In*:
560 Elliot, D.H. & Blaisdell, L.L. (eds) *Contribution to Antarctic Research IV*. Antarctic
561 Research Series, 67. American Geophysical Union, Washington DC, 103-141.
562 Elliot, D. H., Fleming, T. H., Kyle, P. R. & Foland, K. A. 1999. Long-distance transport of
563 magmas in the Jurassic Ferrar large igneous province, Antarctica. *Earth and Planetary*
564 *Science Letters,* **167**, 89–104.
565 Encarnacion, J., Fleming, T.H., Elliot, D.H. & Eales, H. 1996. Synchronous emplacement of
566 Ferrar and Karoo dolerites and the early breakup of Gondwana. *Geology*, **24**, 535-539.
567 Fleming, T.H., Foland, K.A. & Elliot, D.H. 1995. Isotopic and chemical constraints on the
568 crustal evolution and source signature of Ferrar magmas, north Victoria Land, Antarctica.
569 *Contributions to Mineralogy and Petrology*, **121**, 217-236.
570 Fleming, T.H., Heinmann, A., Foland K.A. & Elliot, D.H. 1997. $^{40}Ar/^{39}Ar$ geochronology of
571 Ferrar Dolerite sills from the Transantarctic Mountains, Antarctica: Implications for the age
572 and origin of the Ferrar magmatic province. *Bulletin of the Geological Society of America*,
573 **109**, 533-546.
574 Galerne,C.Y., Nuemann, E-R. & Planke, S. 2008. Emplacement mechanisms of sill complexes:
575 Information from the geochemical architecture of the Golden Valley Sill Complex, South
576 Africa. *Journal of Volcanology and Geothermal Research*, **177**, 425-440.
577 Gibson, S.A., Thompson, R.N., Day, J.A., Humphris, S.E. & Dickin A.P. 2005. Melt-generation
578 associated with the Tristan mantle plume: constraints on the origin of EM-1. *Earth and*
579 *Planetary Science Letters*, **237**, 744-767.
580 Greenway, M. E., 1972. The geology of the Falkland Islands. *British Antarctic Survey Scientific*
581 *Reports*, **76**, 42 pp.
582 Harris, C., Marsh, J.S., Duncan, A.R. & Erlank, A.J. 1990. The Petrogenesis of the Kirwan
583 Basalts of Dronning Maud Land, Antarctica. *Journal of Petrology*, **31**, 341-369.
584 Heinonen, J.S. & Luttinen, A.V. 2008. Jurassic dikes of Vestfjella, western Dronning Maud
585 Land, Antarctica: Geochemical tracing of ferropicrite sources. *Lithos*, **105**, 347-364.
586 Heinonen, J.S., Carlson, R.W. & Luttinen, A.V. 2010. Isotopic (Sr, Nd, Pb, and Os) composition
587 of highly magnesian dikes of Vestfjella, western Dronning Maud Land, Antarctica: A key to
588 the origins of the Jurassic Karoo large igneous province? *Chemical Geology*, **277**, 227-244.

589 Heinonen, J.S., Luttinen, A.V., Riley, T.R. & Nichallik, R.M. 2013. Mixed pyroxenite–
590 peridotite sources for mafic and ultramafic dikes from the Antarctic segment of the Karoo
591 continental flood basalt province. *Lithos*, **177**, 266-380.
592 Heinonen, J.S., Carlson, R.W., Riley, T.R., Luttinen, A.V. & Horan, M.F. 2014. Subduction-
593 modified oceanic crust mixed with a depleted mantle reservoir in the sources of the Karoo
594 continental flood basalt province. *Earth and Planetary Science Letters*, **394**, 229-241.
595 Hergt J. M., Chappell B. W., Mcculloch M. T., McDougall I. & Chivas A. R. 1989. The
596 geochemistry of Jurassic dolerites from Portal Peak, Antarctica. *Contributions to Mineralogy*
597 *and Petrology*, **102**, 298-305.
598 Herzberg, C. & Asimow, P.D. 2008. Petrology of some oceanic island basalts: PRIMELT2.XLS
599 software for primary magma calculation. *Geochemistry, Geophysics, Geosystems*, **9**.
600 Herzberg, C. & Gazel, E. 2009. Petrological evidence for secular cooling in mantle plumes.
601 *Nature*, **458**, 619-623.
602 Hole, M.J. 2015. The generation of continental flood basalts by decompression melting of
603 internally heated mantle. *Geology*, **43**.
604 Hole, M.J., Millett, J.M., Rogers, N.W. & Jolley, D.W. 2015. Rifting and mafic magmatism in
605 the Hebridean basins. *Journal of the Geological Society, London*, **172**, 218-236.
606 Jourdan, F., Féraud, F.G., Bertrand, H., Kampunzu, A.B., Tshoso, Le Gall, G.B., Tiercelin, J.J.
607 & Capiez P, 2004. The Karoo triple junction questioned: evidence from Jurassic and
608 Proterozoic $^{40}Ar/^{39}Ar$ ages and geochemistry of the giant Okavango dyke swarm
609 (Botswana). *Earth and Planetary Science Letters*, **222**, 989-1006.
610 Jourdan, F., Féraud, G., Bertrand, H., Kampunzu, A.B., Tshoso, G., Watkeys, M.K. & Le Gall,
611 B. 2005. Karoo large igneous province: Brevity, origin and relation to mass extinction
612 questioned by new $^{40}Ar/^{39}Ar$ age data. *Geology*, **33**, 745–748.
613 Jourdan, F., Féraud, G., Bertrand, H., Watkeys, M.K. & Renne, P.R. 2007a. Distinct brief
614 major events in the Karoo large igneous province clarified by new $^{40}Ar/^{39}Ar$ ages on the
615 Lesotho basalts. *Lithos*, **98**, 195-209.
616 Jourdan F., Bertrand H., Schärer U., Blichert-Toft J., Feraud G. & Kampunzu A.B. 2007b.
617 Major and trace element and Sr, Nd, Hf, and Pb isotope compositions of the Karoo large
618 igneous province, Botswana-Zimbabwe: lithosphere *vs* mantle plume contribution. *Journal*
619 *of Petrology*, **48**, 1043-1077
620 Keiding, J.K., Trumbull, R.B., Veksler, I.V. & Jerram, D.A. 2011. On the significance of ultra-
621 magnesian olivines in basaltic rocks. *Geology*, **39**, 1095-1098.

622 Lambart, S., Lapporte, D. & Schiano, P. 2013. Markers of the pyroxenite contribution in the
623 major-element compositions of oceanic basalts: Review of the experimental constraints.
624 *Lithos*, **160-161**, 14-36.
625 Luttinen, A.V. & Furnes, H., 2000. Flood basalts of the Vestfjella: Jurassic magmatism across
626 an Arcehan-Proterozoic lithospheric boundary in Dronning Maud Land, Antarctica. *Journal*
627 *of Petrology*, **41**, 1271-1305.
628 Luttinen, A.V., Ramo, O.T. & Huhma, H. 1998. Neodymium and strontium isotope and trace
629 element composition of a Mesozoic CFB suite from Dronning Maud Land, Antarctica:
630 implications for lithosphere and asthenosphere contributions to Karroo magmatism.
631 *Geochimica et Cosmochimica Acta,* **15**, 2701-2714.
632 Macdonald, D.I.M., Gomez-Perez, I., Frnazese, J., Spalleti, L., Lawver, L., Gahagan, L.,
633 Dalziel, I.W.D., Thomas, C.J., Trewin, N.H., Hole, M.J. & Paton, D. 2003. Mesozoic break-
634 up of SW Gondwana: implications for regional hydrocarbon potential of the southern South
635 Atlantic. *Marine & Petroleum Geology*, **20**, 287-308
636 Marsh, J.S., Hooper, P.R., Rehacek, J., Duncan, R.A. & Duncan, A.R. 1997. Stratigraphy and
637 age of Karroo basalts of Lesotho and implications for correlations within the Karroo
638 Igneous Province. In: Mahoney, J.J. & Coffin, M.F. (eds*) Large Igneous Provinces*, A G U
639 Geophysical Monographs, 100, 247-272.
640 McClintock, M., Marsh, J. & White, J.D.L. 2008. Compositionally diverse magmas erupted
641 close together in space and time within a Karoo flood basalt crater complex. *Bulletin of*
642 *Volcanology*, **70**, 923-946.
643 Melluso L., Cucciniello C., Petrone C.M., Lustrino M., Morra V., Tiepolo M. &Vasconcelos L.
644 2008. Petrology of Karoo volcanic rocks in the southern Lebombo monocline,
645 Mozambique. *Journal of African Earth Sciences*, **52**, 139-151.
646 Melluso, L., Hergt, M.J. & Zanetti, A. 2013. The late crystallization stages of low-Ti, low-Fe
647 tholeiitic magmas:Insights from evolved Antarctic and Tasmanian rocks. *Lithos*, **188**, 72-83.
648 Mitchell, C., Ellam, R.M. & Cox, K.G. 1999. Mesozoic dolerite dykes of the Falkland Islands:
649 petrology, petrogenesis and implications for geochemical provinciality in Gondwanaland
650 low-Ti basaltic rocks. *Journal of the Geological Society, London,* **156**, 901-916.
651 Molzahn, M., Reisberg, L. & Wörner, G. 1996. Os, Sr, Nd, Pb, O isotope and trace element
652 data from the Ferrar flood basalts, Antarctica: evidence for an enriched subcontinental
653 lithospheric source. *Earth and Planetary Science Letters*, **144**, 529-546.

654 Muirhead, J.D., Airoldi, G., White, J.L. and Rowland, J.V. 2014. Cracking the lid: Sill-fed
655 dikes are the likely feeders of flood basalt eruptions. *Earth and Planetary Science Letters*,
656 **406**, 187-197.
657 Mussett, A.E. & Taylor, G.K. 1994. ^{40}Ar-^{39}Ar ages for dykes from the Falkland Islands with
658 implications for the break-up of southern Gondwanaland. *Journal of the Geological*
659 *Society, London,* **151**, 79-81.
660 Nielsen, S.B., Stephenson, R.A. & Thomsen, E. 2007. Dynamics of Mid-Palaeocene North
661 Atlantic rifting linked with European intra-plate deformations. *Nature*, **450**, 1071-1074
662 Nuemann, E-R., Svensen, H., Galerne, G.Y. & Planke, S. 2011. Multistage Evolution of
663 Dolerites in the Karoo Large Igneous Province, Central South Africa. *Journal of Petrology*,
664 **52**, 959-984.
665 Putirka, K.D., Perfit, M., Ryerson, F.J. & Jackson, M.G. 2007. Ambient and excess mantle
666 temperatures, olivine thermometry, and active vs. passive upwelling. *Chemical Geology*, **241**,
667 177-206.
668 Richards, P.C., Stone, P., Kimbell, G.S., Mcintosh, W.C. & Phillips, E.R. 2013. Mesozoic
669 magmatism in the Falkland Islands (South Atlantic) and their offshore sedimentary basins.
670 *Journal of Petroleum Geology*, **36**, 61-74.
671 Riley, T.R., Curtis, M.L., Leat, P.T., Watkeys, M.K., Duncan, R.A., Millar, I.L. & Owens, W.H.
672 2006. Overlap of Karoo and Ferrar Magma Types in KwaZulu-Natal, South Africa.
673 *Journal of Petrology*, **47**, 541-566.
674 Riley, T.R., Millar, I.L., Watkeys, M.K., Curtis, M.L., Leat, P.T., Klausen, M.B. & Fanning,
675 C.M. 2004. U-Pb zircon (SHRIMP) ages for the Lemombo rhyolites, South Africa: refining
676 the duration of Karoo magmatism. *Journal of the Geological Society, London,* **161**, 547-
677 550.
678 Sushchevskaya, N.M., Korago, E.A., Belyatsky, B.V. & Sirotkin, A.N. 2009. Evolution of the Karoo-
679 Maud mantle plume in Antarctica and its influence on the magmatism of the early stages of Indian
680 ocean opening. *Geochemistry International*, **47**, 1-17.
681 Stone, P., Kimbell, G.S. & Richards, P.C. 2009. Rotation of the Falklands microplate reassessed
682 after recognition of discrete Jurassic and Cretaceous dyke swarms. *Petroleum Geoscience*,
683 **15**, 279-287.
684 Stone, P., Richards, P.C., Kimbell, G.S., Esser, R.P.,& Reeves, D. 2008 Cretaceous dykes
685 discovered in the Falkland Islands: implications for regional tectonics in the South Atlantic.
686 *Journal of the Geological Society, London,* **165**, 1-4

687 Storey, B.C., Hole, M.J., Pankhurst, R.J., Millar, I.L. & Vennum, W. 1988. Middle Jurassic
688 within-plate granites in West Anratctica and their bearing on the break-up of Gondwana.
689 *Journal of the Geological Society, London*, **145**, 999-1007.
690 Storey, B.C., Alabaster, T., Hole, M.J., Pankhurst, R.J. & Wever, H. 1992. Role of subduction-
691 plate boundary forces during the initial stages of Gondwana break-up: Evidence from the
692 proto-Pacific margin of Antarctica. *In:* Storey, B. C., Alabaster, T. & Pankhurst, R. J. (eds)
693 *Magmatism and the causes of Continental Break-Up* Geological Society, London, Special
694 Publications, **64,** 149-163.
695 Sweeney R. J., Duncan A. R., Erlank A. J. 1994. Geochemistry and Petrogenesis of Central
696 Lebombo basalts of the Karoo igneous province. *Journal of Petrology*, **35** 95-125.
697 Sun, S-S. & Mcdonough, W. F. 1989. Chemical and isotopic systematics of oceanic basalts:
698 implications for mantle composition and processes. In: Saunders, A.D. & Norry, M.J.,
699 (eds). *Magmatism in the ocean basins*. Geological Society, London, Special Publications,
700 **42,** 313-345.
701 Sushchevskaya, N. M., Belyatskii, B. V., Leichenov, G. L. & Laiba A. A. 2009. Evolution of the
702 Karoo-Maud plume in Antarctica and its influence on the magmatism of the early stages of
703 Indian Ocean opening. *Geochemistry International*, **47**, 1-17
704 Thistlewood, L., Leat, P. T., Millar, I.L., Storey, B.C. & Vaughan, A. P. M. 1997. Basement
705 Geology and Palaeozic-Mesozoic mafic dykes from the Cape Meredith Complex, Falkland
706 Islands: a record of repeated intracontinental extension. *Geological Magazine,* **134**, 355-
707 367.
708 Thompson, R.N., Gibson, S.A., Dickin, A.P. & Smith, P.M. 2001. Early Cretaceous basalt and
709 picrate dykes of the Southern Etendeka region, NW Namibia: windows into the role of the
710 Tristan plume in Parana-Etendeka magmatism. *Journal of Petrology*, **42**, 2049-2081.
711 Wilhelm, S. & Wörner, G. 1996. Crystal size distribution in Jurassic Ferrar flows and sills
712 (Victoria Land, Antarctica): evidence for processes of cooling, nucleation and
713 crystallization. *Contributions to Mineralogy and Petrology*, **125**, 1-15.
714 Williamson, I.T. & Bell, B.R. 2012. The Staffa Lava Formation: graben-related volcanism,
715 associated sedimentation and landscape character during the early development of the
716 Palaeogene Mull Lava Field, NW Scotland. *Scottish Journal of Geology*, **48**, 1-46.
717

718 **Figure Captions**

719 Figure 1. a) Reconstruction of Southern Gondwana immediately prior to break-up at c. 180 Ma.
720 MEB, Maurice Ewing Bank; EWM, Ellsworth-Whitmore Mountains; AP, Antarctic Peninsula;
721 SA, South Africa; SAM, South America; ANT, Antarctica. Position of the Weddell, Limpopo
722 and Lower Zambesi triple junctions are from Elliot & Fleming (2000). Ar-Ar ages, this study
723 and Stone *et al.* (2009). After Macdonald *et al.* (2003). b) Map showing the distribution of
724 break-up related igneous rocks of Antarctica. Fine pecked lines are contours for depth to the
725 Moho (Baranov & Morelli 2013), and the grey pecked lines encompass the region of the Ferrar
726 Igneous Province according to Elliot (2013).

727 Figure 2. Map of the Falkland Islands showing the distribution of magnetic anomalies and main
728 trends of dyke swarms. Solid or pecked lines do not necessarily represent continuous exposure
729 of dykes. Inset; azimuths of Dykes in the South Harbour area of West Falkland. The rectangle at
730 South Harbour is the area covered by the map in the supplementary material, which gives the
731 sample locations in that area. After Stone *et al.* (2009) and Richards *et al.* (2013). Ar-Ar ages
732 (this study, Stone *et al.* 2008; 2009) and sample locations in East Falkland which are mentioned
733 in the text, are indicated.

734 Figure 3. Ar-Ar step-heating spectrum for plagioclase in sample WI-5.

735 Figure 4. a) Major (weight %) and trace element (in ppm) variations *versus* MgO weight % in
736 Falkland Islands dykes. Filled dots, Port Sussex Creek type (PST) NE-SW two-pyroxene
737 dolerites; open triangles, E-W olivine dolerite dykes; open squares, Lively Island dyke; filled
738 squares, Mount Alice-type (MAT) dykes; open dots, low TiO_2 DIT intrusions; filled diamonds,
739 high TiO_2 DIT intrusions; open diamonds, evolved sheets from the South Harbour-Dyke Island
740 transect (Dyke Island Type; DIT); crosses, Pony's Pass N-S Cretaceous dyke (Stone *et al.*
741 2008). Data from this study, Mitchell *et al.* (1999) and Thistlewood *et al.* (1997).

742 Figure 5. a) Pyroxene end-member compositions represented in the quadrilateral system
743 Enstatite - Ferrosilite – Wollastonite for Falkland Islands intrusions (this study and Mitchell *et*
744 *al.* 1999) and dolerites from the Transantarctic Mountains (Elliot 1995; Demarchi *et al.* 2001).
745 MFCT, Mount Fazio Chemical Type; SPCT, Scarab Peak Chemical Type; NVL, Northern
746 Victoria Land.

747 Figure 6. Ti/Zr *versus* SiO_2 and TiO_2 *versus* MgO, for Falkland Islands dykes (symbols as for
748 Fig. 4), Ferrar LIP dolerites and Dronning Maud land volcanic rocks. Data sources;
749 Transantarctic Mountains and Theron Mountains; Hergt *et al.* (1989), Brewer *et al.* (1992),
750 Elliot *et al.* (1995), Fleming *et al.* (1995), Molzahn *et al.* (1996), Wörner *et al.* (1996), Antonini

et al. (1999), Elliot *et al.* (1999), Elliot & Fleming (2004), Wilhelm & Worner (1996). Dronning Maud Land; Heinonen & Luttinen (2008); Luttinen *et al.* (1998), Luttinen & Furnes (2000), Heinonen *et al.* (2010; 2013; 2014). Kirwanveggan; Harris *et al.* (1990).

Figure 7. a) Chondrite-normalized REE profiles for representative samples of a) PST, MAT and E-W intrusions; b) DIT intrusions.

Figure 8. a) to d) Multi-element ORB-normalized (Sun & McDonough 1989) variation diagrams for Falkland Islands dykes. Comparable basalts from other regions of the low TiO_2 Gondwana LIP are shown by grey lines. Sample SA.6.1 (South Africa), Riley *et al.* (2006); VF111-85, CT3 basalt, Dronning Maud Land (Luttinen & Furnes 2000); 47206-3, low TiO_2 tholeiite from Schirmacher Oasis, Dronning Maud Land (Sushchevskaya *et al.* 2009); Average SPCT from Elliot *et al.* (1995).

Figure 9. a) εNd_{182} *versus* $^{87}Sr/^{86}Sr_{182}$; b) $^{207}Pb/^{204}Pb$ *versus* $^{206}Pb/^{204}Pb$ for Falkland Islands dykes. c) εNd_{182} *versus* $^{207}Pb/^{204}Pb$ for Falkland Islands intrusions. Symbols as for Fig. 4. Data sources this study, Mitchell *et al.* (1999) and Thistlewood *et al.* (1997).

Figure. 10 a) and b) εNd_{182} and $^{87}Sr/^{86}Sr_{182}$ *versus* MgO; c) εNd_{182} versus Th/Ta and d) $^{87}Sr/^{86}Sr_{182}$ *versus* 1/Sr for Falkland Islands intrusions. Symbols as for Fig. 4 except grey dots are for the lowest reported Th/Ta for Ferrar dolerites (Fleming *et al.* 1995). Parameters for the AFC mixing line are given in Table 4 with % AFC given on the mixing line.

Fig. 11. a) εNd_{182} *versus* $^{87}Sr/^{86}Sr_{182}$ for Falkland Islands PST intrusions (filled dots) Karoo low TiO_2 volcanic rocks (open circles), Dronning Maud Land CT1 (open triangles), CT2 (filled diamonds) and CT3 (filled triangles) basalts. Details of the parameters used in generating the three AFC mixing lines (CT1, PST-1 and PST-2) are given in Table 4. Each cross represents 1% AFC. Data sources for Karoo Province; Galerne *et al.* (2008); McClintock *et al*. (2008); Neumann *et al.* (2011).

Figure 12. a) CaO *versus* MgO (weight %) for Falkland Islands intrusions (black dots PST; grey dots, DIT; grey squares MAT; grey triangles, E-W) and Dronnning Maud Land high MgO, silica-oversaturated CT1 basalts (circles). The dividing line between melts derived from peridotite and pyroxenite sources is taken from Herzberg & Asimow (2008). Lines with crosses and arrows represent the effect of accumulation of the phase indicated on the composition of PST basalt NEF9, with each cross representing 5% accumulation. b) Cr (ppm) *versus* SiO_2 for Falkland Islands intrusions (symbols as for Fig. 4) and high-Mg andesites from Mt Shasta (crosses; Baker *et al.* 1994).

Figure 13. a) Olivine equilibration temperatures (°C) *versus* Mg# of liquid in equilibrium with olivine for Ahlmannryggen dykes (filled dots; Heinonen & Luttinen 2008), Vestfjella high TiO_2 ferropicrite (filled triangles; Heinonen *et al.* 2013), Etendeka picrite (open squares; Kieding *et al.* 2011) and Falklands Islands MAT (star in circle) and E-W (open triangles) intrusions. Olivine equilibration temperatures have been calculated according to the scheme of Putirka *et al*. (2007). Vertical lines connecting points for Ahlmannryggen samples are calculated equilibration temperatures for different olivine phenocrysts in individual whole-rock samples. Figures in italics are T_P from melt inclusions for Etendeka samples plotted in Fig. 13b (Kieding *et al.* 2011). b) T_P calculated from melt inclusions in ultra-magnesian olivines from the Etendeka Provice *versus* olivine equilibration temperatures for the same samples. Data from Keiding *et al.* (2011). c) Inferred temperature-pressure conditions at which fractional melting terminated for calculated primary magmas from Dronning Maud Land, the Karoo Province of southern Africa, Ferrar dolerites of Antarcitca and picrites of the Etendeka Province of western Africa. The diagram was constructed following the methods of Herzberg and Gazel (2009) and Hole (2015). Samples with MgO > 20 weight % are shown schematically following an adiabatic pathway for T_P = 1640°C. The diagonally shaded box on the temperature axis is the range of olivine equilibration temperatures, calculated at 0 GPa, for olivine in ferro-picrite dykes from Dronning Maud following the method of Putirka et al. (2007), and the box labelled 'MAT & E-W' is the same calculations for MAT and E-W intrusions. Adiabatic melting paths are labelled with mantle potential temperature. 2σ error bars are from Hole (2015).

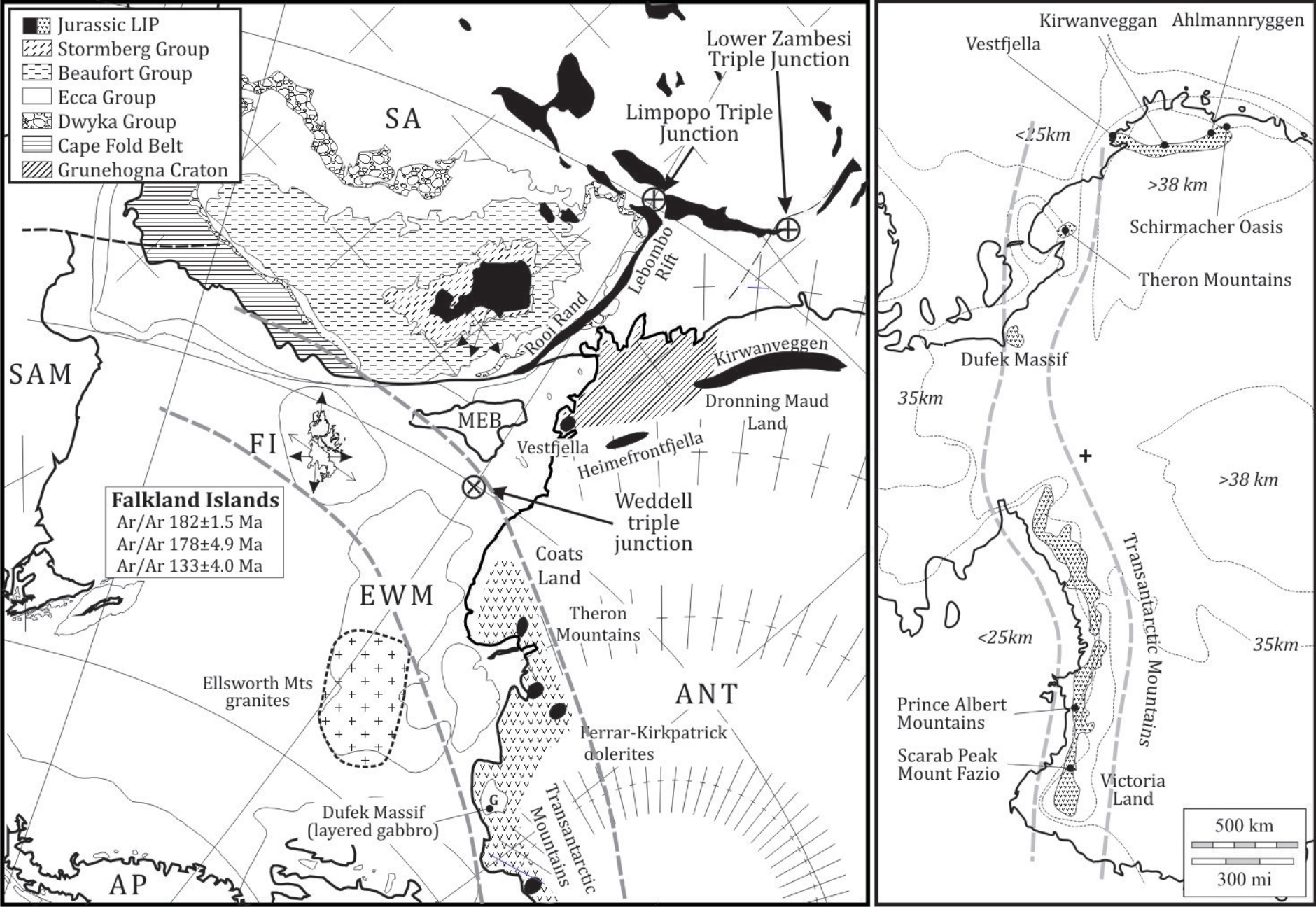
Jurassic LIP
Stormberg Group
Beaufort Group
Ecca Group
Dwyka Group
Cape Fold Belt
Grunehogna Craton
SA
SAM
FI
EWM
ANT
AP
Lower Zambesi Triple Junction
Limpopo Triple Junction
Lebombo Rift
Rooi Rand
Kirwanveggen
Dronning Maud Land
MEB
Vestfjella
Heimefrontfjella
Weddell triple junction
Coats Land
Theron Mountains
Falkland Islands
Ar/Ar 182±1.5 Ma
Ar/Ar 178±4.9 Ma
Ar/Ar 133±4.0 Ma
Ellsworth Mts granites
Ferrar-Kirkpatrick dolerites
Dufek Massif (layered gabbro)
G
Transantarctic Mountains
Kirwanveggan
Ahlmannryggen
Vestfjella
<25km
>38 km
Schirmacher Oasis
Theron Mountains
Dufek Massif
35km
>38 km
<25km
35km
Transantarctic Mountains
Prince Albert Mountains
Scarab Peak
Mount Fazio
Victoria Land
500 km
300 mi

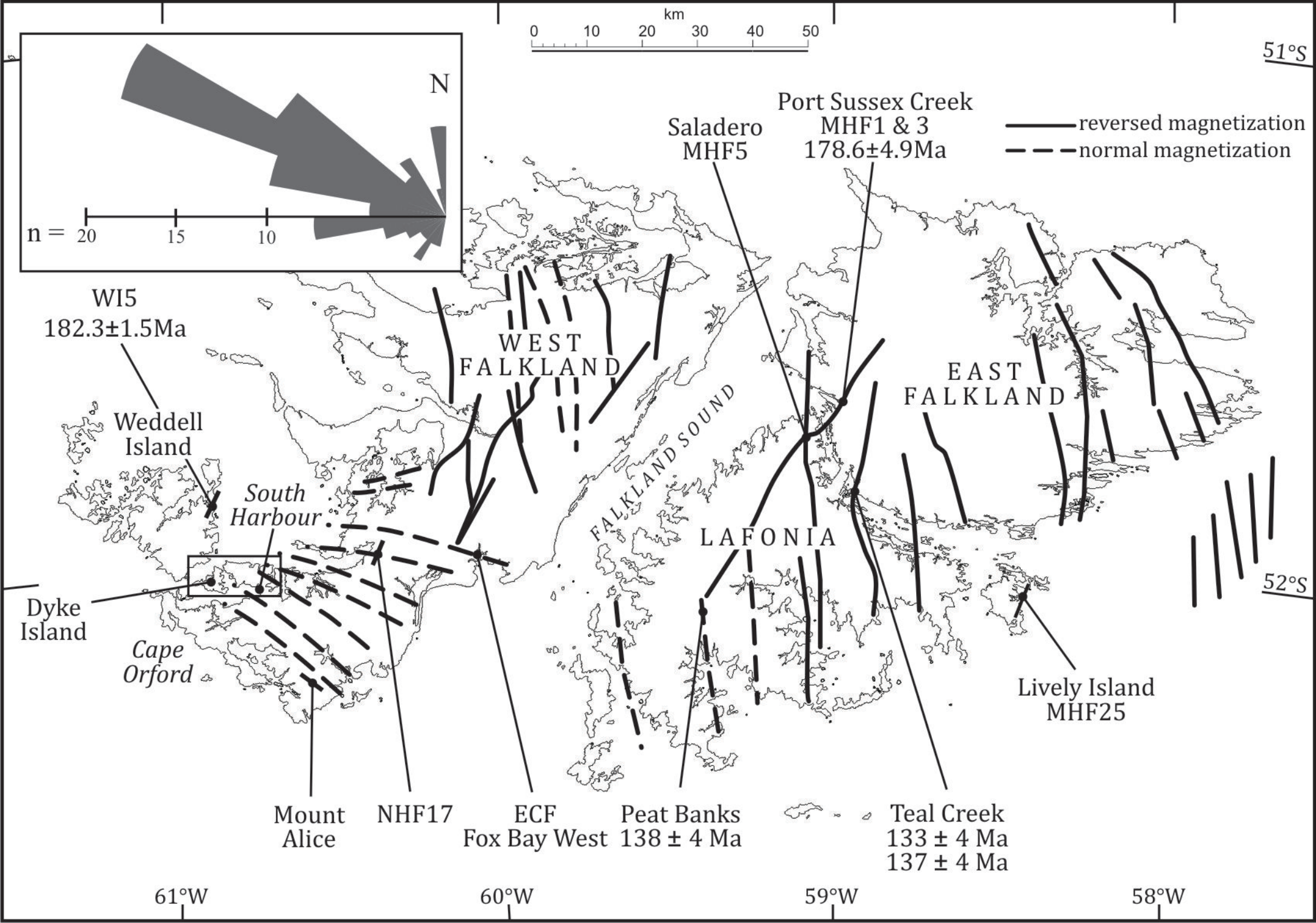
km
0
10
20
30
40
50
N
n =
20
15
10
51°S
52°S
61°W
60°W
59°W
58°W
reversed magnetization
normal magnetization
Saladero
MHF5
Port Sussex Creek
MHF1 & 3
178.6±4.9Ma
WI5
182.3±1.5Ma
WEST
FALKLAND
EAST
FALKLAND
FALKLAND SOUND
LAFONIA
Weddell
Island
South
Harbour
Dyke
Island
Cape
Orford
Lively Island
MHF25
Mount
Alice
NHF17
ECF
Fox Bay West
Peat Banks
138 ± 4 Ma
Teal Creek
133 ± 4 Ma
137 ± 4 Ma

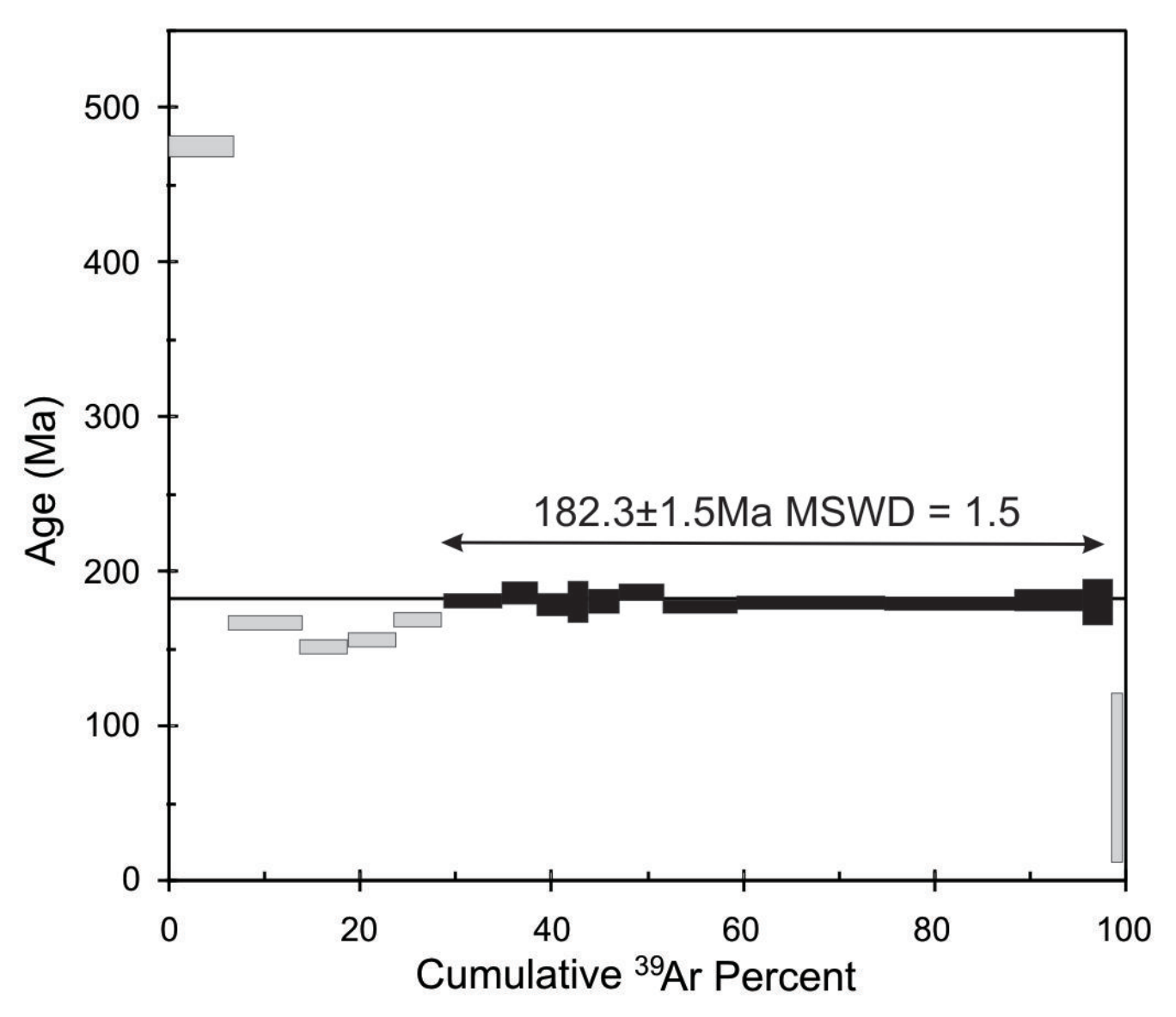
500
400
300
200
100
0
Age (Ma)
182.3±1.5Ma MSWD = 1.5
0
20
40
60
80
100
Cumulative 39Ar Percent

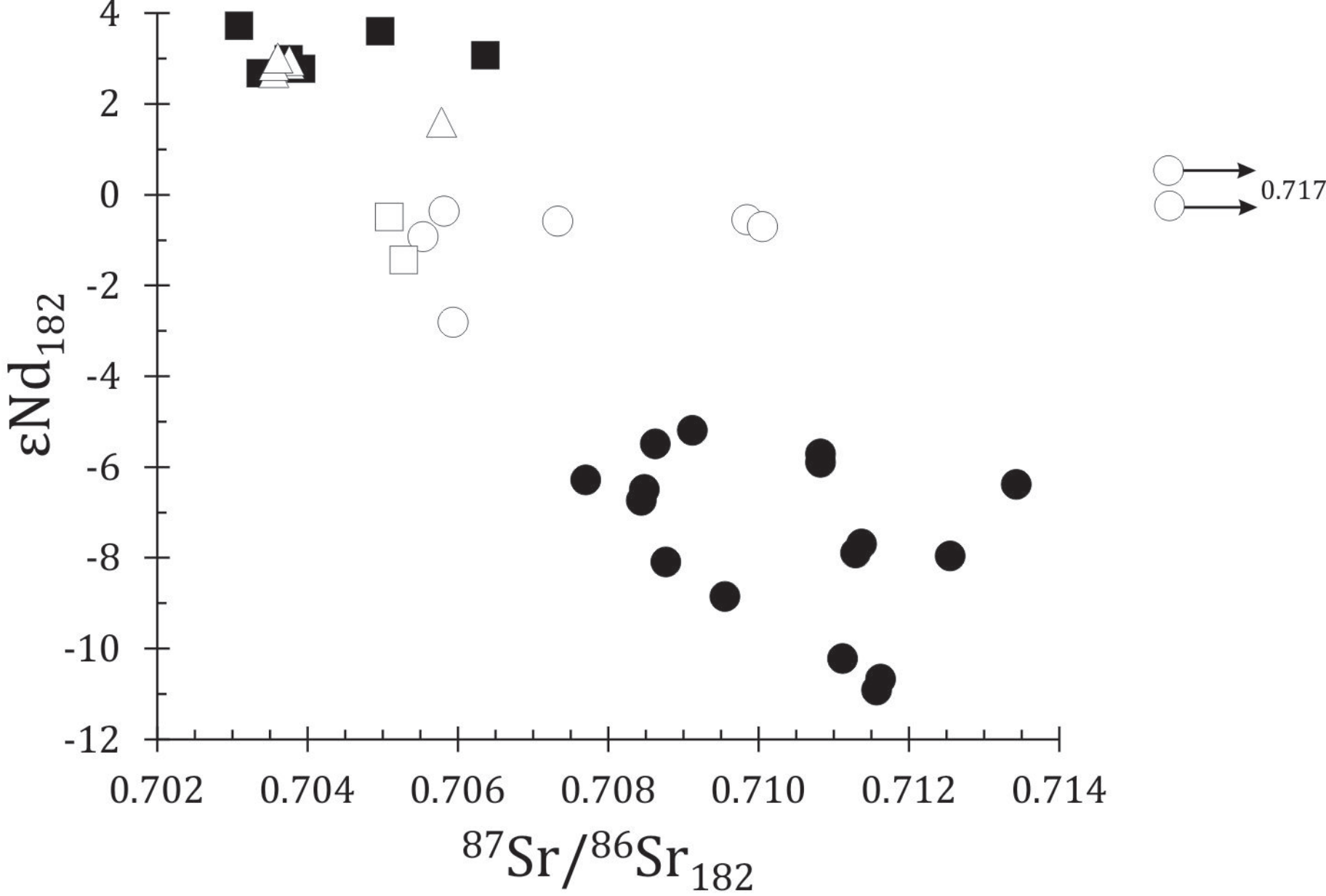
εNd182
87Sr/86Sr182
0.717
207Pb/204Pb
206Pb/204Pb
Geochron
NHRL
εNd182
207Pb/204Pb

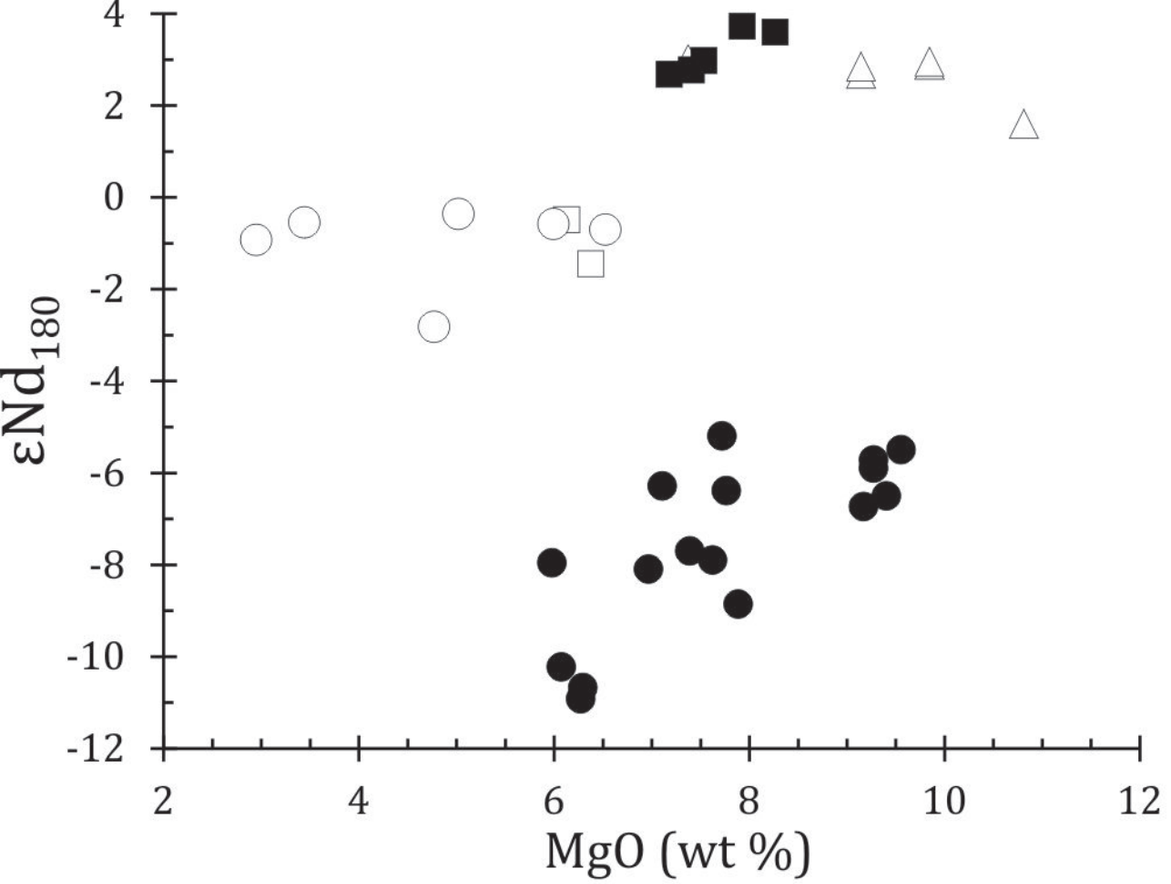
4
2
0
-2
-4
-6
-8
-10
-12
εNd180
2
4
6
8
10
12
MgO (wt %)

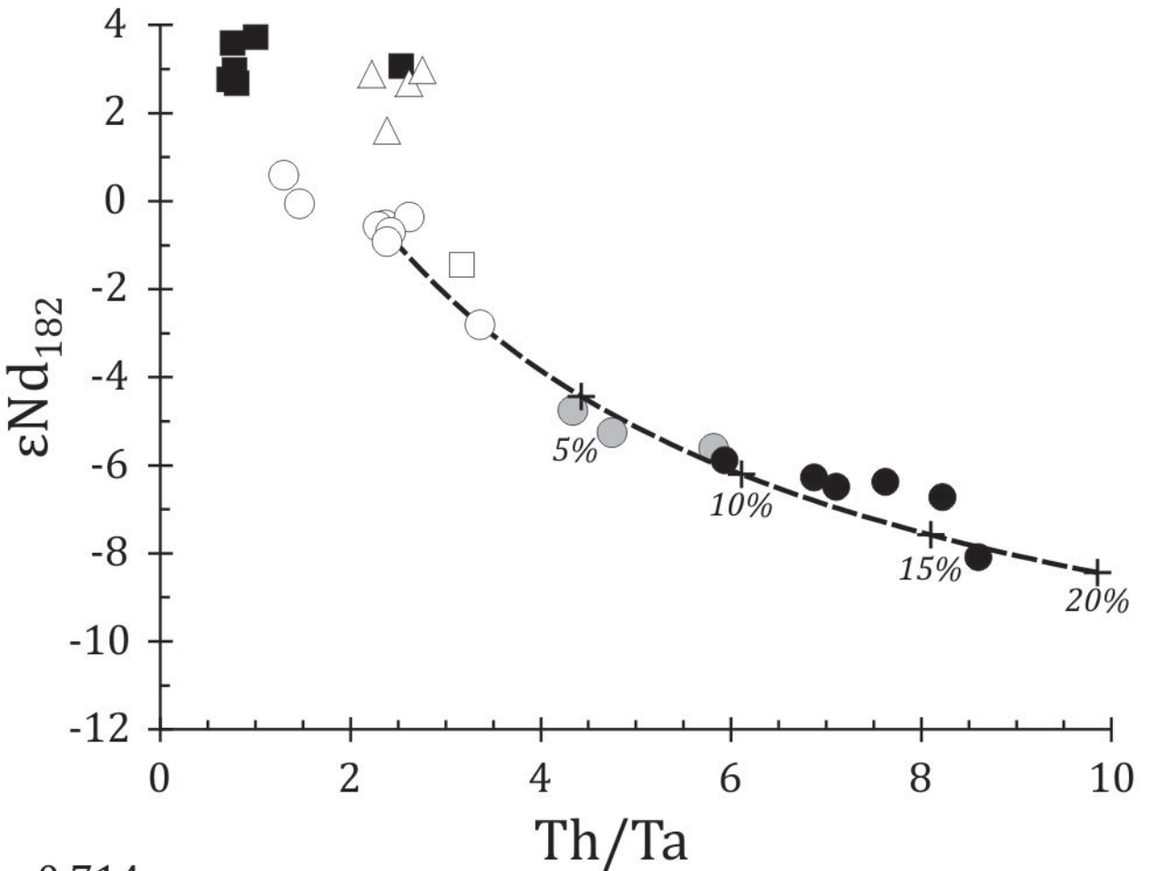
4
2
0
-2
-4
-6
-8
-10
-12
εNd182
5%
10%
15%
20%
0
2
4
6
8
10
Th/Ta

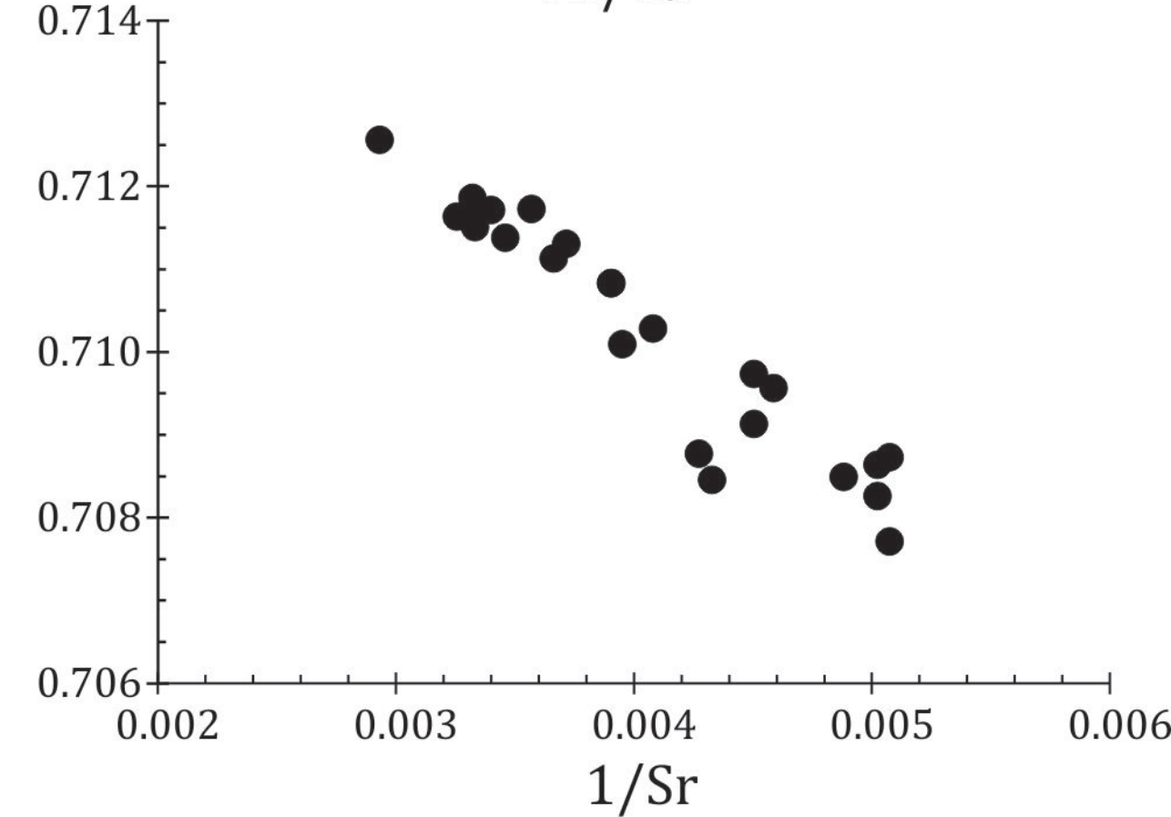
0.714
0.712
0.710
0.708
0.706
0.002
0.003
0.004
0.005
0.006
1/Sr

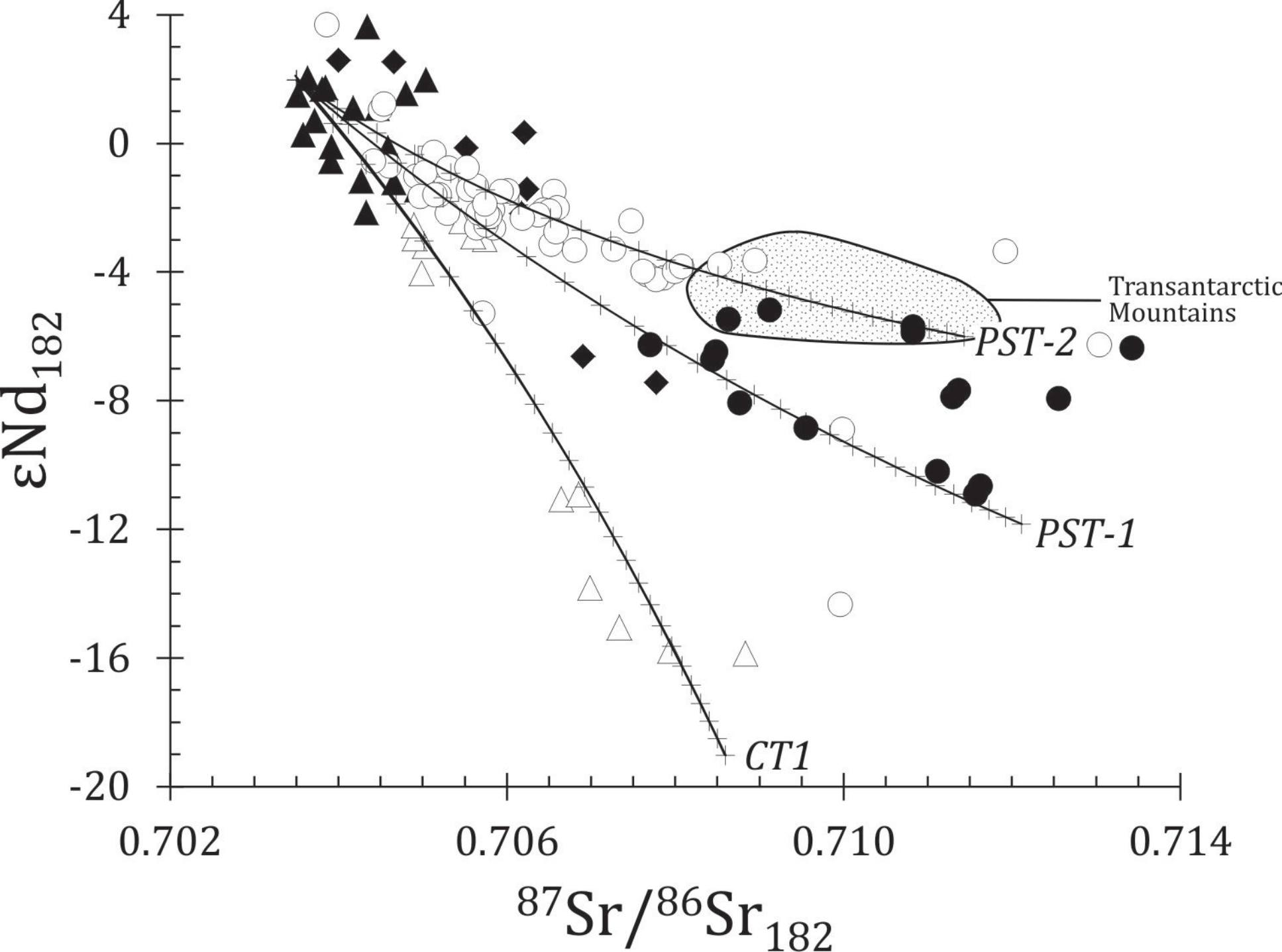
4
0
-4
-8
-12
-16
-20
εNd182
0.702
0.706
0.710
0.714
87Sr/86Sr182
Transantarctic
Mountains
PST-2
PST-1
CT1

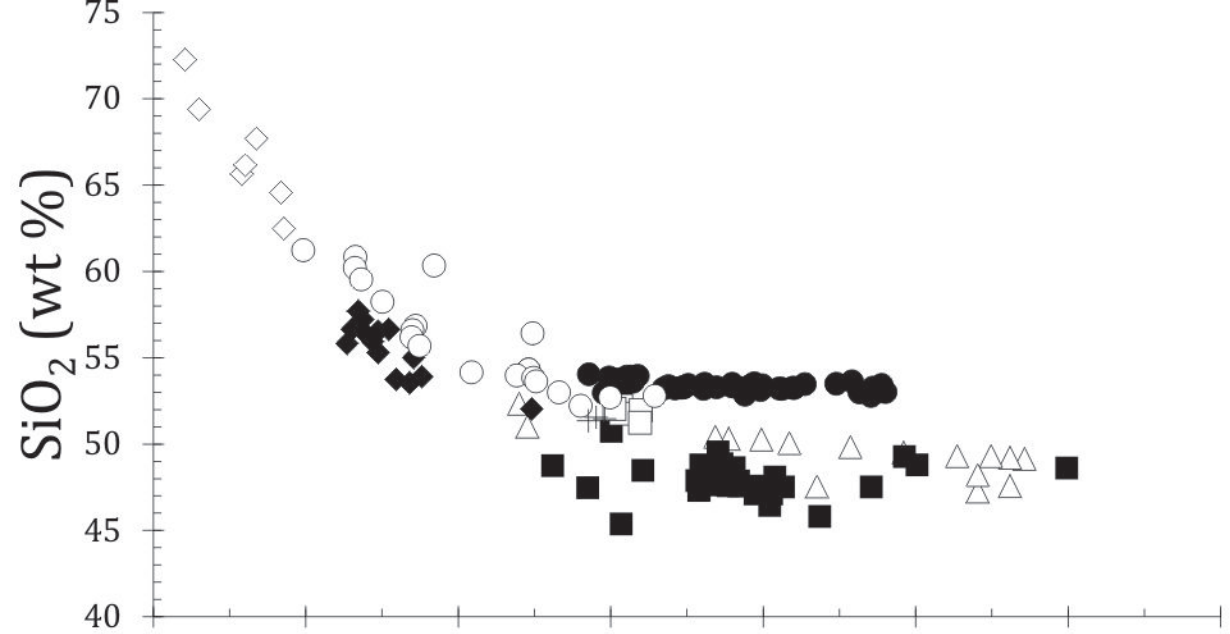
SiO2 (wt %)
75
70
65
60
55
50
45
40

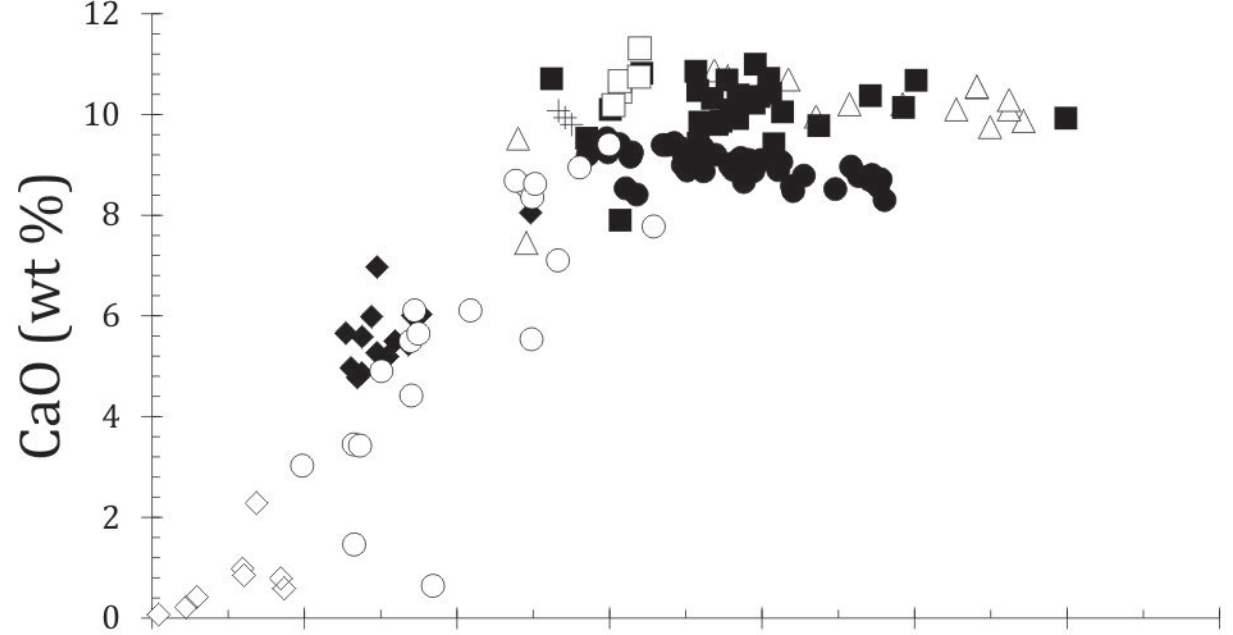
CaO (wt %)
12
10
8
6
4
2
0

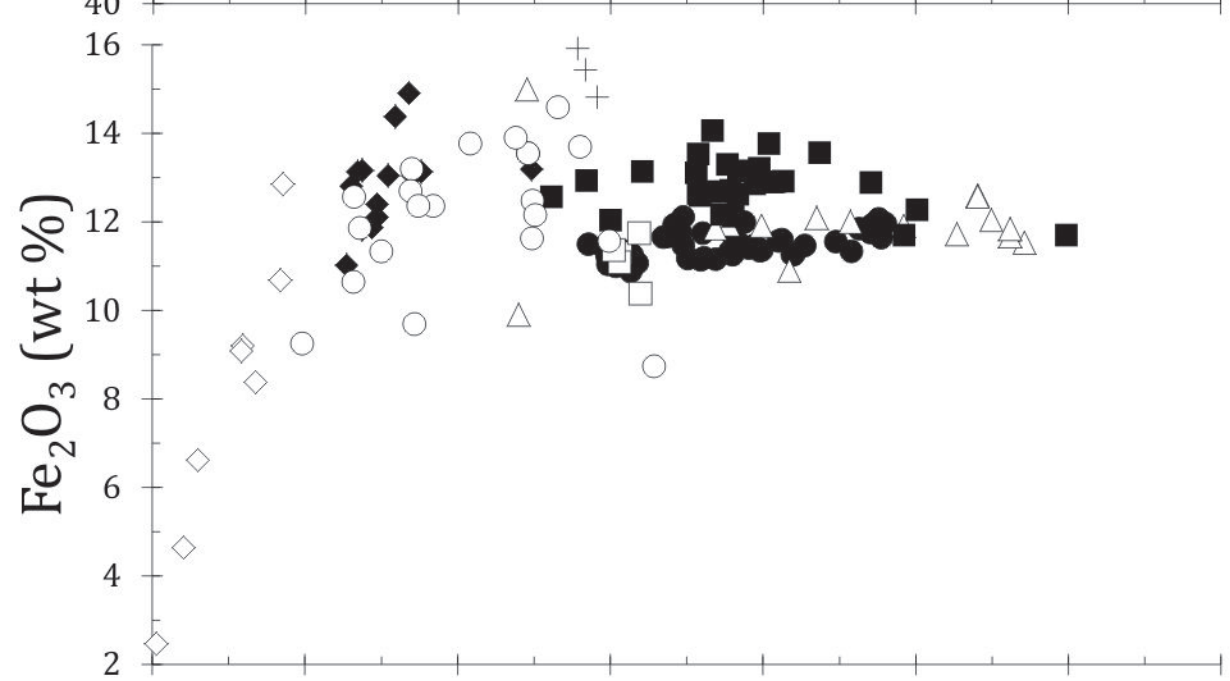
Fe2O3 (wt %)
16
14
12
10
8
6
4
2

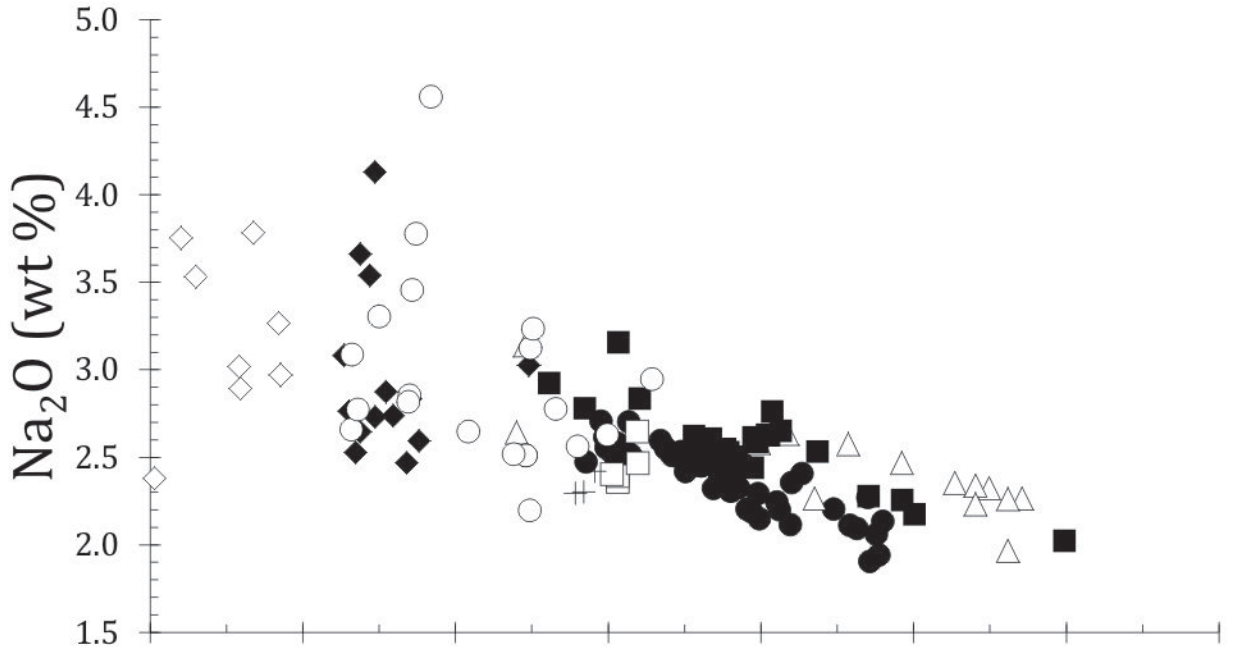
Na2O (wt %)
5.0
4.5
4.0
3.5
3.0
2.5
2.0
1.5

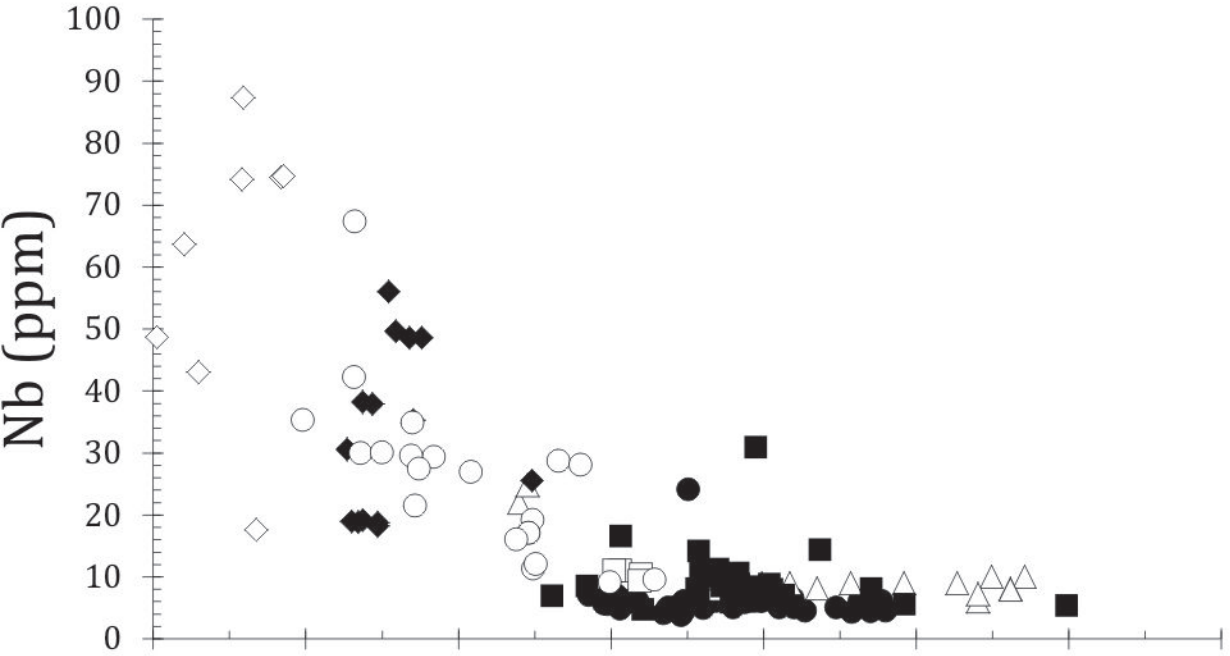
Nb (ppm)
100
90
80
70
60
50
40
30
20
10
0

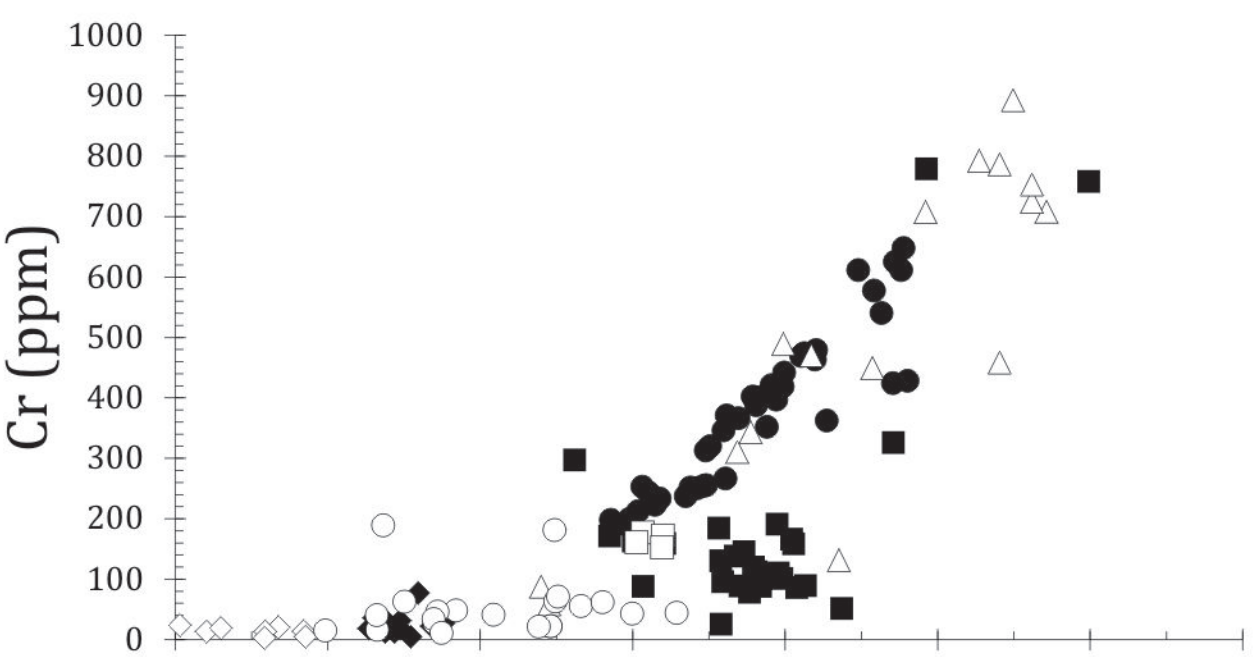
Cr (ppm)
1000
900
800
700
600
500
400
300
200
100
0

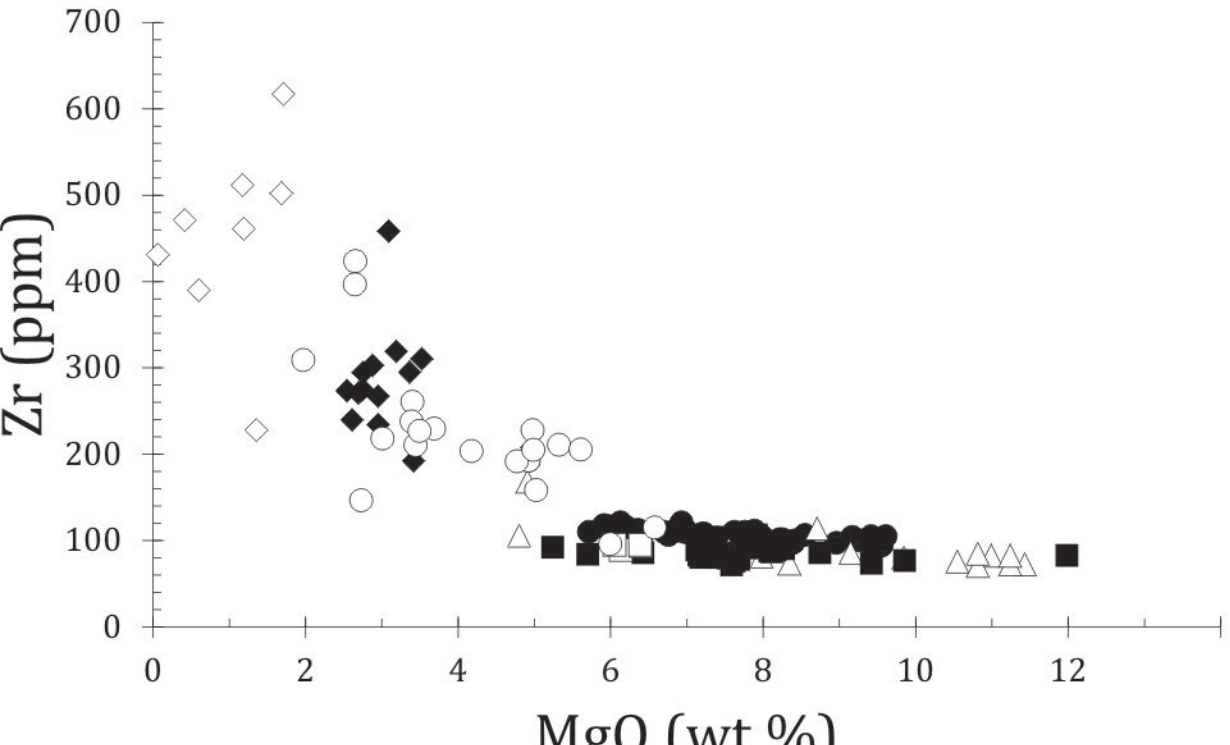
Zr (ppm)
700
600
500
400
300
200
100
0
0
2
4
6
8
10
12
MgO (wt %)

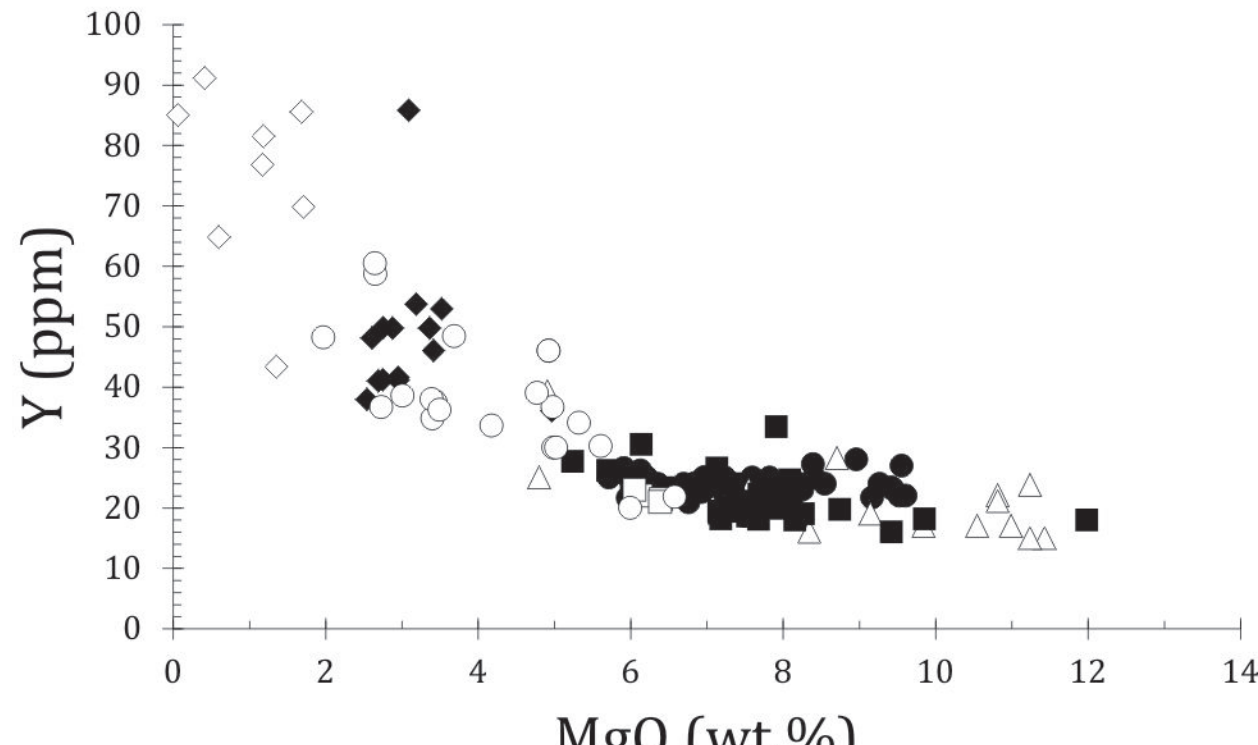
Y (ppm)
100
90
80
70
60
50
40
30
20
10
0
0
2
4
6
8
10
12
14
MgO (wt %)

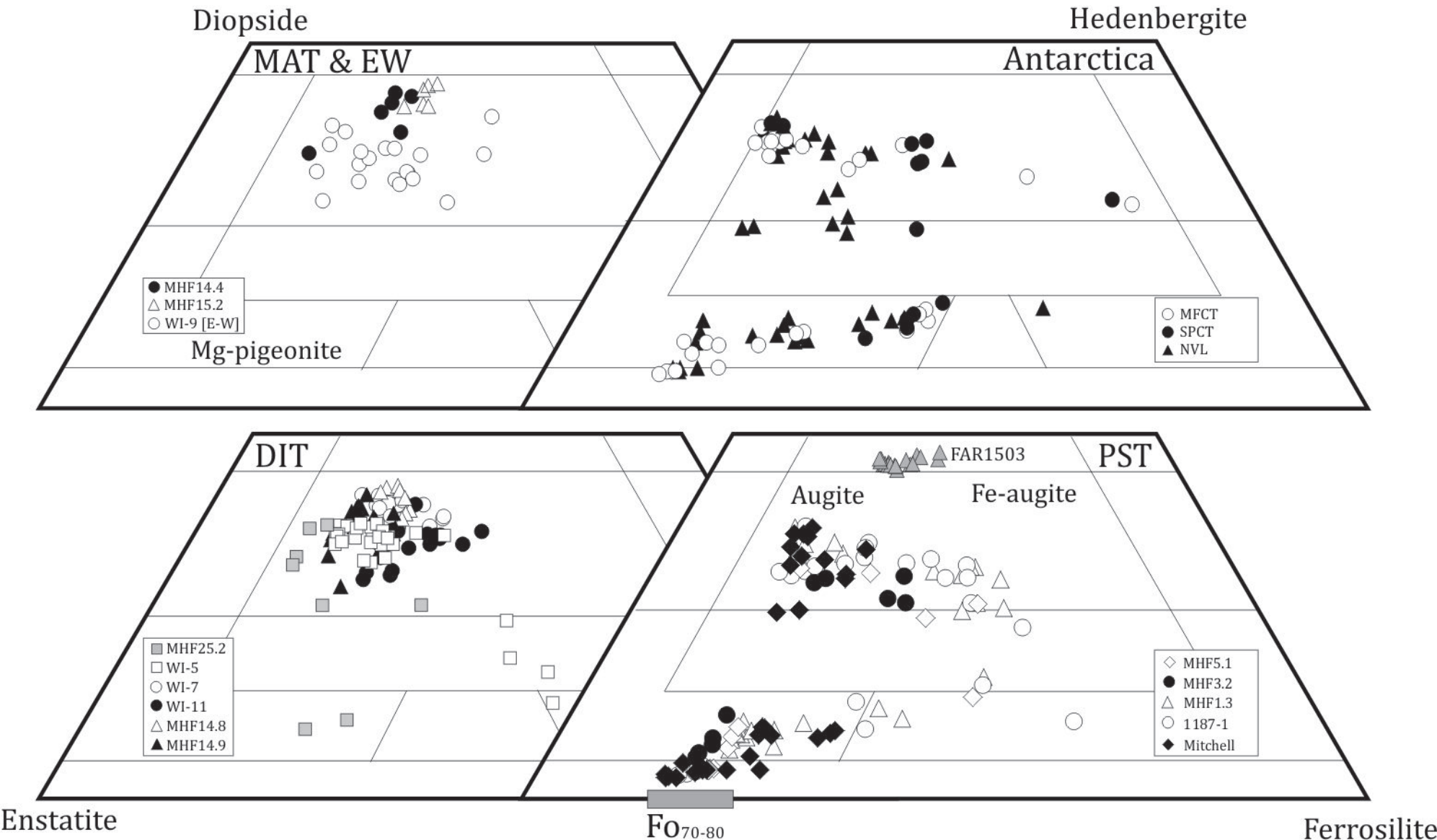
Diopside
Hedenbergite
MAT & EW
Antarctica
MHF14.4
MHF15.2
WI-9 [E-W]
Mg-pigeonite
MFCT
SPCT
NVL
DIT
PST
FAR1503
Augite
Fe-augite
MHF25.2
WI-5
WI-7
WI-11
MHF14.8
MHF14.9
MHF5.1
MHF3.2
MHF1.3
1187-1
Mitchell
Enstatite
Fo70-80
Ferrosilite

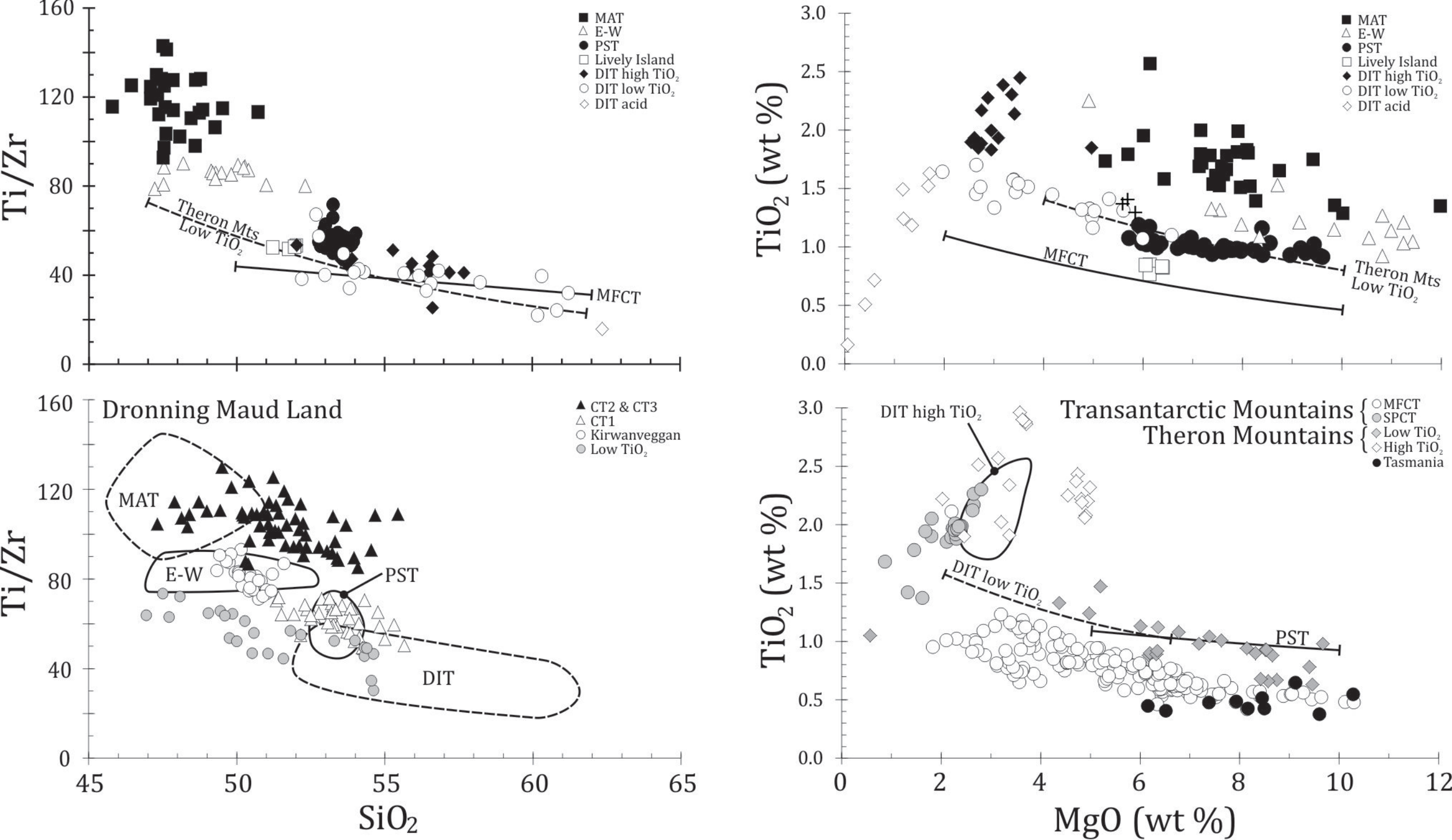
Ti/Zr
MAT
E-W
PST
Lively Island
DIT high TiO2
DIT low TiO2
DIT acid
Theron Mts
Low TiO2
MFCT
TiO2 (wt %)
Dronning Maud Land
CT2 & CT3
CT1
Kirwanveggan
Low TiO2
MAT
E-W
PST
DIT
SiO2
Transantarctic Mountains
Theron Mountains
MFCT
SPCT
Low TiO2
High TiO2
Tasmania
DIT high TiO2
DIT low TiO2
PST
MgO (wt %)

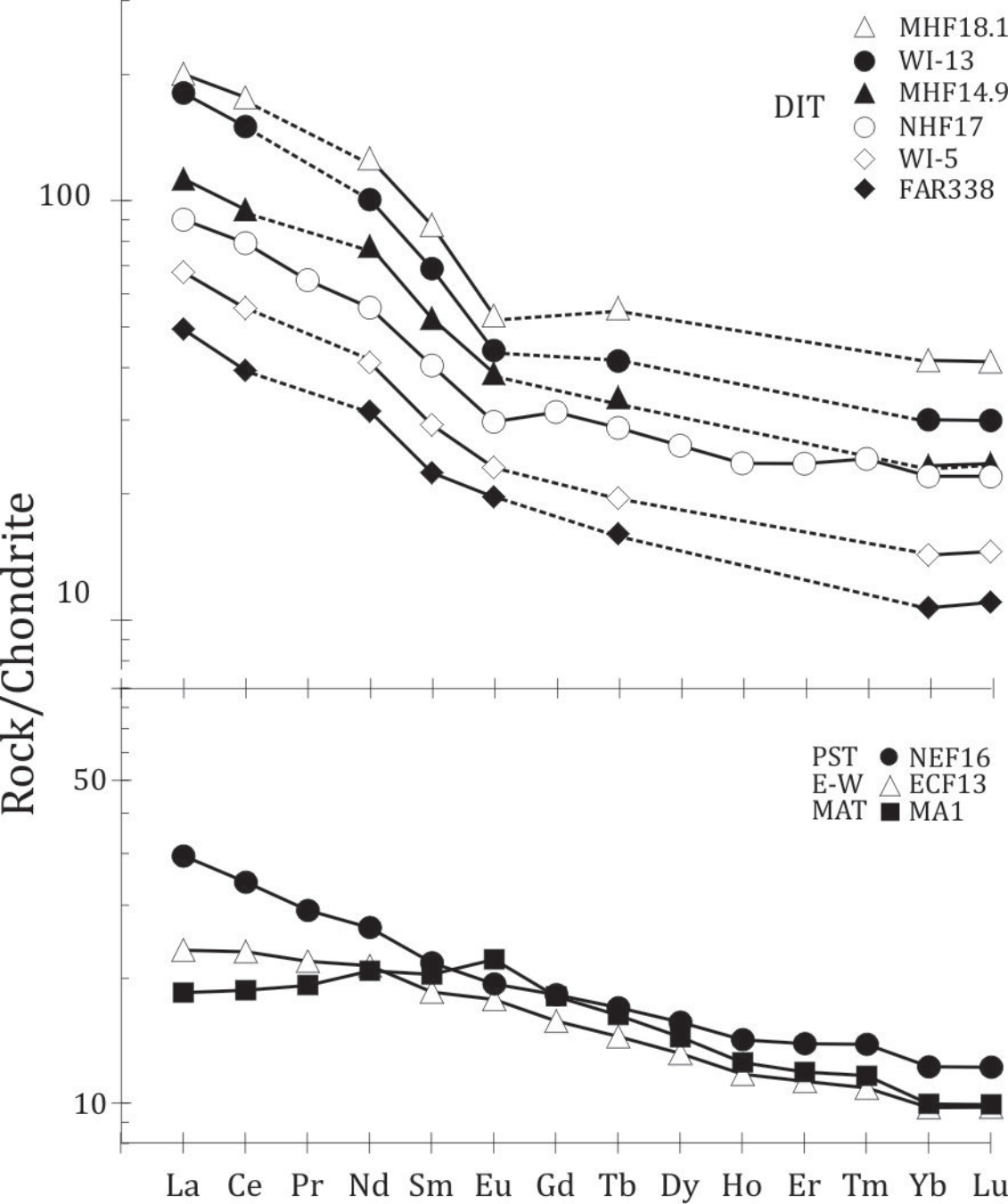
MHF18.1
WI-13
MHF14.9
NHF17
WI-5
FAR338
DIT
100
10
Rock/Chondrite
PST
E-W
MAT
NEF16
ECF13
MA1
50
10
La
Ce
Pr
Nd
Sm
Eu
Gd
Tb
Dy
Ho
Er
Tm
Yb
Lu

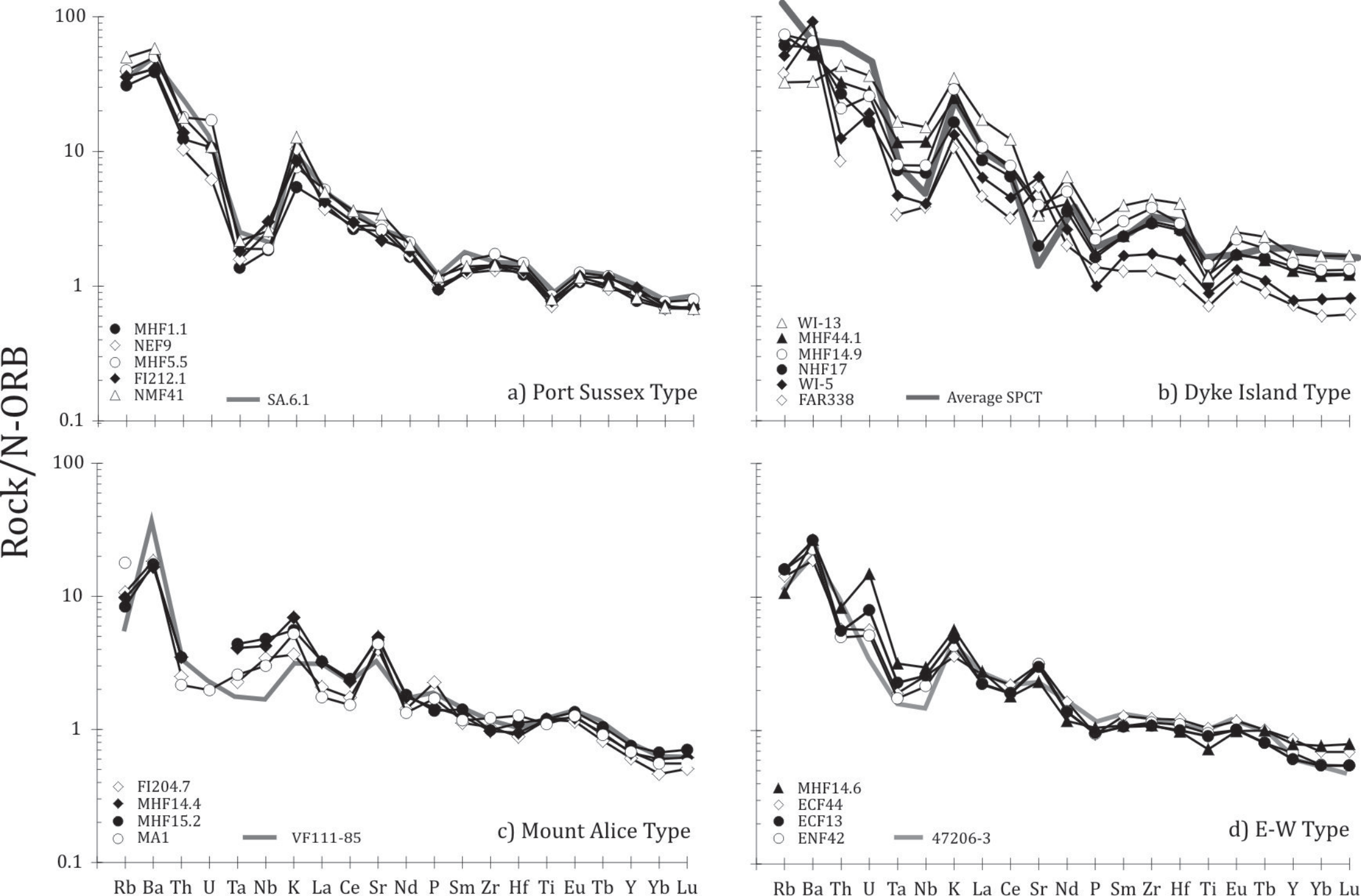
Rock/N-ORB
100
10
1
0.1
MHF1.1
NEF9
MHF5.5
FI212.1
NMF41
SA.6.1
a) Port Sussex Type
WI-13
MHF44.1
MHF14.9
NHF17
WI-5
FAR338
Average SPCT
b) Dyke Island Type
FI204.7
MHF14.4
MHF15.2
MA1
VF111-85
c) Mount Alice Type
MHF14.6
ECF44
ECF13
ENF42
47206-3
d) E-W Type
Rb Ba Th U Ta Nb K La Ce Sr Nd P Sm Zr Hf Ti Eu Tb Y Yb Lu

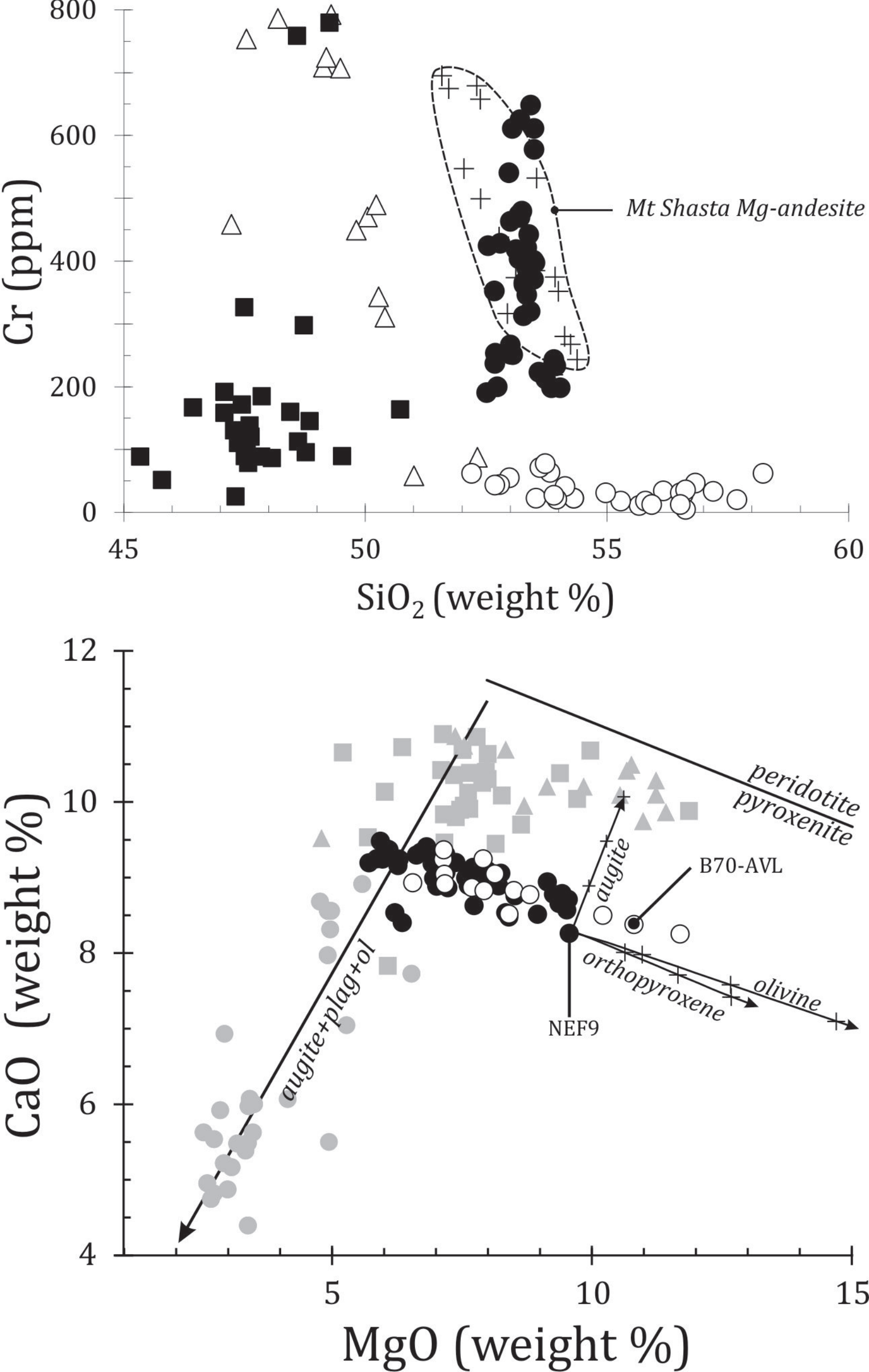
Cr (ppm)
800
600
400
200
0
45
50
55
60
SiO2 (weight %)
Mt Shasta Mg-andesite
CaO (weight %)
12
10
8
6
4
5
10
15
MgO (weight %)
peridotite
pyroxenite
B70-AVL
augite
augite+plag+ol
orthopyroxene
olivine
NEF9

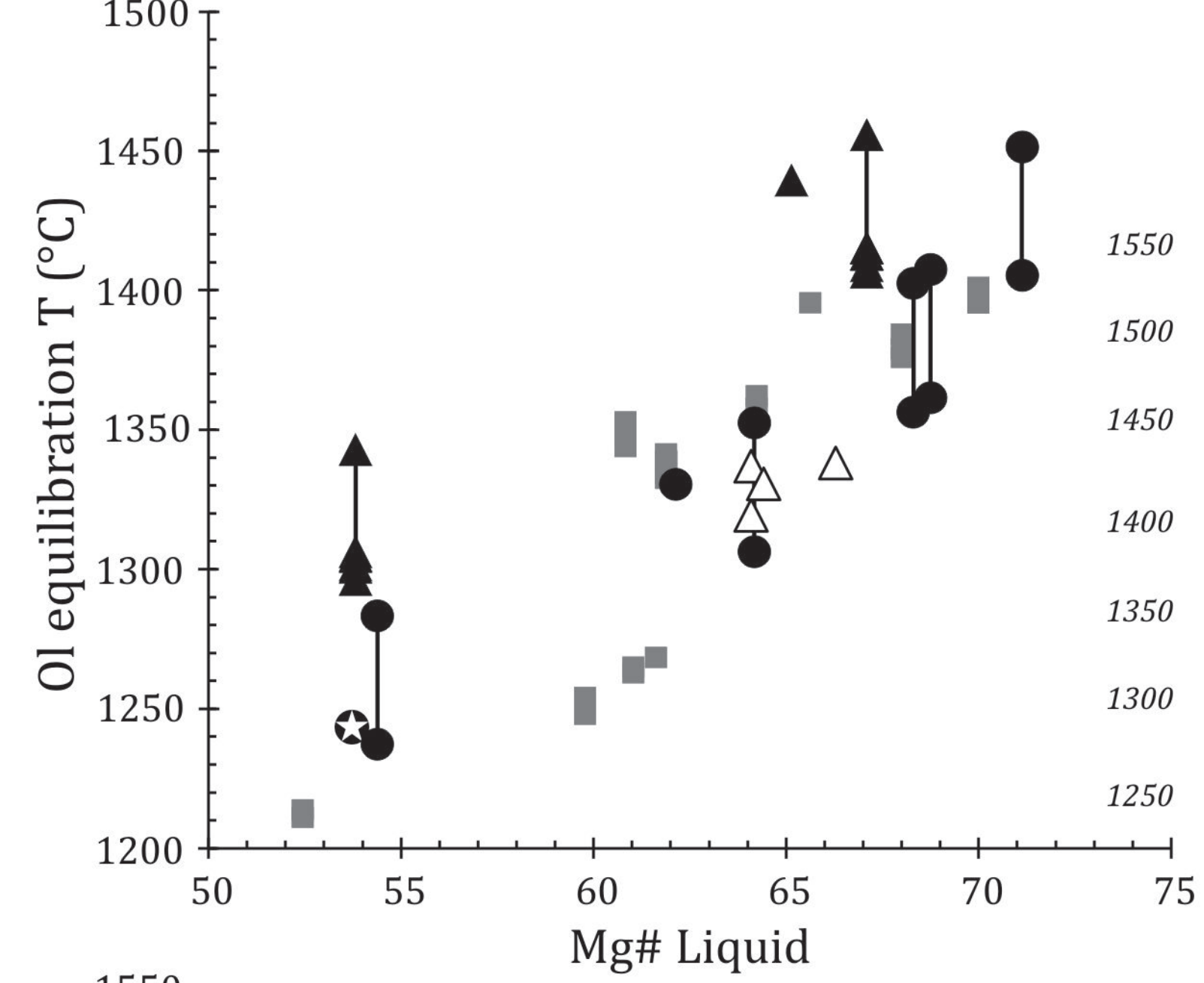
Ol equilibration T (°C)
1500
1450
1400
1350
1300
1250
1200
50
55
60
65
70
75
Mg# Liquid
1550
1500
1450
1400
1350
1300
1250

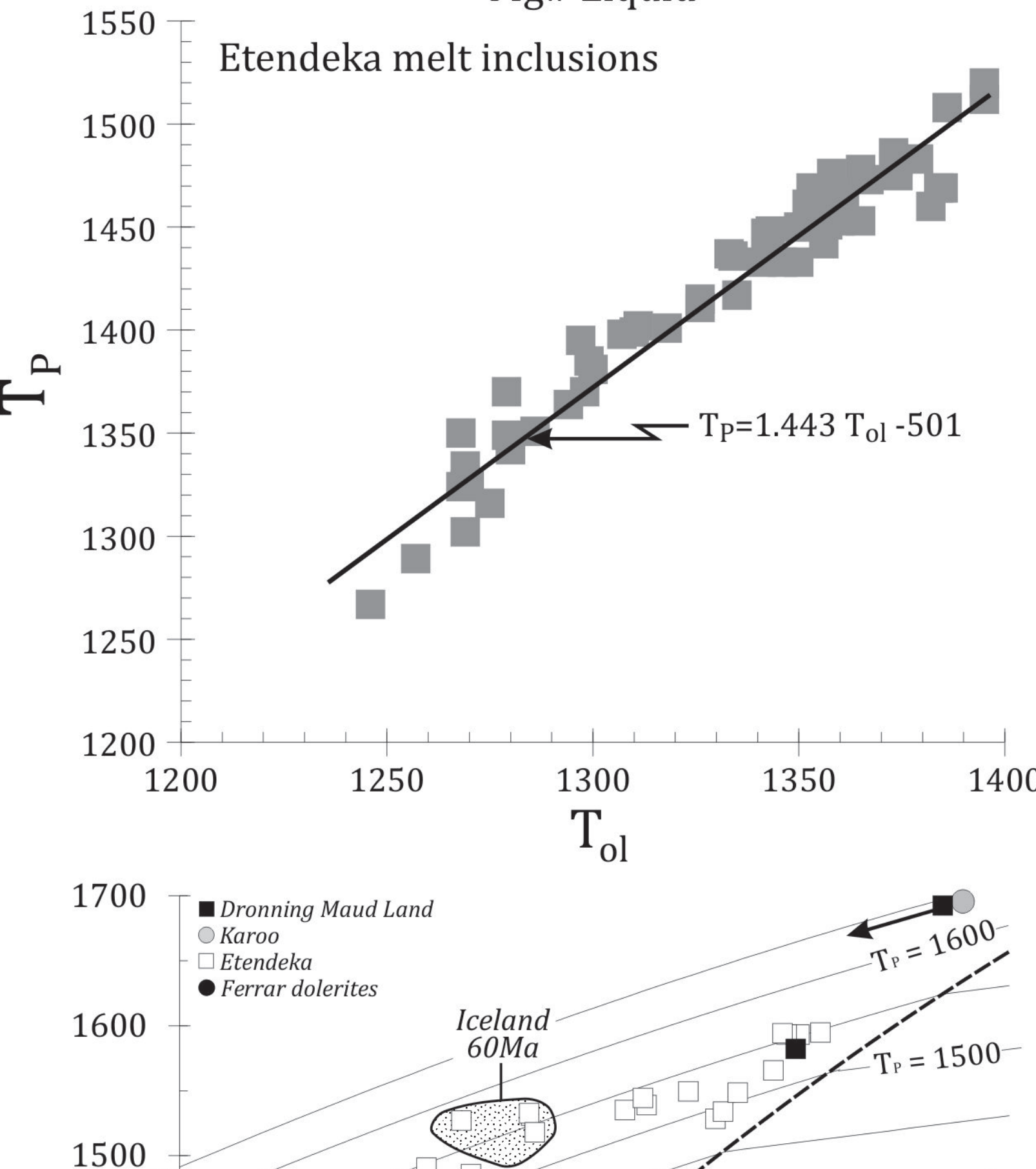
Etendeka melt inclusions
T_P=1.443 T_{ol} -501
T_P
T_{ol}
1550
1500
1450
1400
1350
1300
1250
1200
1200
1250
1300
1350
1400

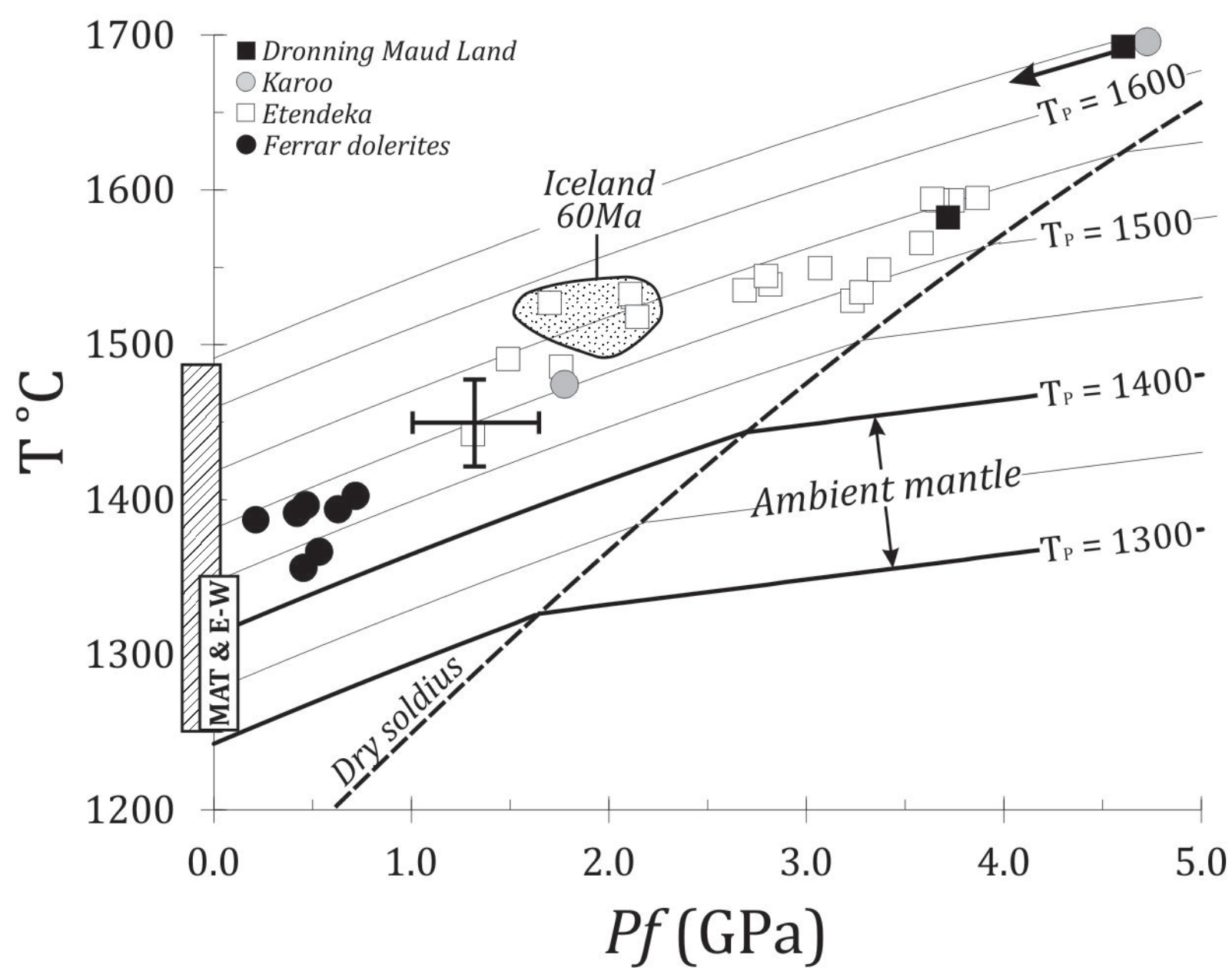
Dronning Maud Land
Karoo
Etendeka
Ferrar dolerites
Iceland
60Ma
MAT & E-W
Dry soldius
Ambient mantle
T_P = 1600
T_P = 1500
T_P = 1400
T_P = 1300
T °C
Pf (GPa)
1700
1600
1500
1400
1300
1200
0.0
1.0
2.0
3.0
4.0
5.0

Sample	MHF15.2	MHF14.4	MHF15.1	MA1	MHF41.3	MHF18.1	MHF44.1	MHF18.3	NHF17
	MAT	MAT	MAT	MAT	DIT Acid	DIT Acid	DIT Acid	DIT	DIT
SiO_2	45.92	47.40	48.56	47.51	68.92	64.11	55.49	53.24	53.97
TiO_2	1.81	1.52	1.71	1.39	0.71	1.51	1.54	1.30	1.32
Al_2O_3	15.70	16.39	16.71	16.45	15.03	15.96	15.28	15.01	13.27
Fe_2O_3	13.60	13.23	12.52	12.91	6.57	10.61	12.31	12.05	13.88
MnO	0.16	0.17	0.21	0.20	0.10	0.06	0.22	0.12	0.22
MgO	8.00	7.51	7.15	8.27	0.60	1.67	3.48	4.99	4.77
CaO	10.59	10.65	9.80	10.05	0.40	0.75	5.63	8.56	8.68
K_2O	2.59	2.53	2.53	2.65	3.51	3.25	3.76	3.21	2.52
P_2O_5	0.30	0.05	0.17	0.38	3.29	0.75	1.78	0.66	1.18
Na_2O	0.20	0.17	0.19	0.20	0.21	0.69	0.20	0.17	0.19
TOTAL	98.87	99.63	99.56		99.34	99.36	99.69	99.30	
Loss	1.5	1.90	2.25		3.44	3.30	1.56	3.64	
Rb	4.7	5.5	2.0	10	59.6	20.5	40	17.6	34
Sr	424	444	381	396	715	1204	324	367	178
Nb	11.2	9.9	10.7	7	72	74.4	27.4	12.0	16
Zr	80	79	80	90	620	502	226	158	192
Y	21.1	18.6	18.2	19	64.8	85.5	36.2	30.0	39
Cr	89	78	95	89	19	13	11	71	21
Ni	119	102	121	116	2.0	8	6	95	10
Ba	110	105	103	827	862	2939	528	199	371
La	8.1	8.0	7.9	4.37	68.9	47.5	27.0	15.7	21.36
Ce	18.0	17.2	18.3	11.45	140.0	108	55.6	32.6	48.50
Pr				1.83					6.14
Nd	13.3	12.8	13.8	9.73	69.3	58.9	29.7	20.5	25.93
Sm	3.72	3.32	3.78	3.08	13.60	13.2	6.18	5.32	6.12
Eu	1.38	1.25	1.42	1.29	3.41	3.09	1.77	1.63	1.72
Gd				3.72					6.46
Tb	0.7	0.63	0.72	0.61	2.06	2.07	1.04	0.94	1.07
Dy				3.66					6.62
Ho				0.71					1.34
Er				1.97					3.91
Tm				0.30					0.62
Yb	2.05	1.83	2.04	1.69	7.47	7.07	3.62	2.81	3.74
Lu	0.32	0.28	0.33	0.23	1.11	1.05	0.55	0.44	0.0.56
Th	0.42	0.42	0.48	0.26	6.54	5.6	3.90	1.49	3.19
U				0.09	2.10	2.2	1.30	0.9	0.77
Ta	0.58	0.54	0.6	0.3	4.47	4.32	1.54	0.57	0.95
Hf	2.28	1.94	2.26	2.60	13.80	11.7	5.53	3.78	5.29
Pb				1.07					13.83
Cs	0.3	0.35	0.2		0.20	0.3	0.38	0.4	
Co	48.2	42.60	49.3		7.40	12.5	29.4	50.6	
Sc	28.9	25.40	28.6		13.30	16.3	23.7	15.8	
$^{87}Sr/^{86}Sr$	0.70400	0.70385±1	0.70342		0.71745	0.71720	0.70730	0.70618	
± 2SE	±14	7	±15		±14	±17	± 17	±17	
$^{87}Sr/^{86}Sr_{182}$	0.70392	0.70375	0.70338	0.70497	0.7168	0.71716	0.70633	0.70581	0.70594
$^{143}Nd/^{144}Nd$	0.512747	0.512743	0.512738		0.512542	0.512595	0.512561	0.512572	
± 2SE	±6	±17	±6		±7	±7	± 6	±5	
$^{143}Nd/^{144}Nd_{182}$	0.512537	0.512548	0.512532	0.512588	0.512398	0.512427	0.512405	0.512377	0.512259
εNd_{190}	2.8	3.0	2.7	3.6	-0.1	0.6	0.1	-0.4	-2.8
$^{206}Pb/^{204}Pb$	19.152±6	17.858±7	18.131±7	17.91	18.393±6	18.326±8		18.430±8	
$^{207}Pb/^{204}Pb$	15.656±5	15.476±6	15.579±7	15.50	15.529±6	15.576±8		15.633±7	
$^{208}Pb/^{204}Pb$	38.464±13	37.425±18	37.762±16	37.57	37.583±12	37.880±20		37.944±2	

Sample	WI-5	MHF14.9	WI-3	1187-1	#1503	NEF9	NMF41	MHF1.1	MHF5.5
	DIT	DIT	DIT	PST	PST	PST	PST	PST	PST
SiO_2	52.44	56.06	60.88	52.67	53.20	52.41	53.59	53.49	53.01
TiO_2	1.10	1.81	1.63	0.97	1.02	0.89	1.02	0.99	1.07
Al_2O_3	19.53	14.30	15.24	14.00	12.90	15.69	14.87	13.15	13.90
Fe_2O_3	8.66	12.28	9.19	11.94	11.90	11.50	11.25	11.29	12.03
MnO	0.12	0.18	0.12	0.14	0.14	0.13	0.17	0.13	0.16
MgO	6.54	2.93	1.96	7.74	9.43	5.96	6.29	9.15	6.93
CaO	7.73	5.22	3.01	8.63	8.79	9.35	9.24	8.94	9.18
K_2O	2.92	4.10	5.74	2.45	1.90	2.61	2.52	2.10	2.52
P_2O_5	0.22	2.06	1.10	0.98	0.46	0.77	0.92	0.40	0.55
Na_2O	0.11	0.25	0.59	0.18	0.16	0.16	0.14	0.11	0.13
Total	99.36	99.20	99.45	99.70	99.90			99.75	99.48
Loss	3.28	4.12	2.81	1.50	0.50			1.26	2.62
Rb	29	40.8	18.2	33.1	14.2	22	28	17	22
Sr	582	358	302	533	205	256	307	232	234
Nb	9.5	18.2	35.2	5.8	4.9	6	6	4.3	4.4
Zr	115	267	309	110	93	97	106	104	113
Y	21.8	41.1	48.2	23.9	23.1	25	23	22	25.1
Cr	44	31	15	352	625	589	223	577	255
Ni	7	20	2.0	100	170	133	75	146	91
Ba	153	1409	207	nd	nd	1235	365	250	316
La	16.0	26.7	42.8	11.6	9.3	9.35	12.42	10.10	12.90
Ce	33.9	58.3	91.9	25.1	20.1	20.87	27.19	19.90	24.90
Pr						2.77	3.44		
Nd	19.2	36.4	47.0	14.7	12.3	12.37	14.64	12.00	15.3
Sm	4.41	7.92	10.4	3.58	3.15	3.29	3.68	3.34	4.06
Eu	1.34	2.25	2.55	1.22	1.05	1.12	1.19	1.09	1.28
Gd						3.76	4.16		
Tb	0.73	1.27	1.55	0.72	0.63	0.64	0.68	0.77	0.79
Dy						3.98	4.20		
Ho						0.80	0.83		
Er						2.30	2.37		
Tm						0.35	0.36		
Yb	2.43	3.97	5.11	2.14	1.93	2.08	2.12	2.09	2.33
Lu	0.37	0.60	0.76	0.33	0.28	0.31	0.31	0.32	0.36
Th	1.50	2.48	5.17	1.83	1.35	1.24	2.14	1.48	2.15
U	0.90	1.20	1.70	0.80	0.50	0.29	0.51	0.5	0.8
Ta	0.62	1.04	2.19	0.24	0.19	0.21	0.29	0.18	0.25
Hf	3.18	5.94	8.35	2.73	2.33	2.6	2.86	2.49	3.03
Pb						5.55	4.93		
Cs	0.28	0.56	0.20	0.42	0.29			2.24	0.74
Co	23.20	35.00	16.70	43.30	47.30			50.8	42.9
Sc	18.80	24.70	18.40	25.70	26.60			27.8	28.2
$^{87}Sr/^{86}Sr$	0.71042	0.70730	0.71029	0.71448	0.70900			0.70900	0.70948
± 2 SE	±6	± 17	± 23	±1	± 2			± 18	± 17
$^{87}Sr/^{86}Sr_{182}$	0.71004	0.7055	0.70983	0.71400	0.70846	0.71083		0.70842	0.70873
$^{143}Nd/^{144}Nd$	0.512533	0.512561	0.512535	0.512252	0.512255			0.512259	0.512181
± 2SE	±8	± 6	± 7	±7	± 0			± 6	± 6
$^{143}Nd/^{144}Nd_{182}$	0.51236	0.512349	0.512369	0.512069	0.512063	0.512367		0.51205	0.511981
εNd_{190}	-0.7	-0.9	-0.6	-6.4	-6.5	-5.7		-6.7	-8.1
$^{206}Pb/^{204}Pb$	18.067±9		18.016±10		17.826±11	17.86		18.394 ±8	18.057± 7
$^{207}Pb/^{204}Pb$	15.512±8		15.508±10		15.622 ±8	15.61		15.658± 8	15.643 ±8
$^{208}Pb/^{204}Pb$	37.425±12		37.492±26		38.044±19	37.97		38.143±20	38.246±16

Sample	ECF13	ECF42	ECF44	MHF14.6	MHF25.1
	EW	EW	EW	EW	Lively
SiO_2	49.49	49.82	50.40	47.02	51.76
TiO_2	1.15	1.21	1.32	0.92	0.82
Al_2O_3	14.30	14.47	15.22	14.79	15.94
Fe_2O_3	11.91	11.99	11.85	12.54	10.33
MnO	0.17	0.18	0.02	0.19	0.13
MgO	9.85	9.14	7.38	10.77	6.38
CaO	10.20	10.20	10.87	10.49	11.27
K_2O	2.47	2.58	2.57	2.33	2.46
P_2O_5	0.36	0.31	0.26	0.41	0.73
Na_2O	0.11	0.11	0.11	0.11	0.17
Total				99.57	99.63
Loss				2.20	1.88
Rb	9	9	8	6	10.9
Sr	269	282	283	208	231
Nb	6	5	6	6.9	10.3
Zr	80	85	91	81	93
Y	17	19	24	22.1	21.4
Cr	707	449	310	458	172
Ni	236	174	113	254	63
Ba	167	144	126	208	205
La	5.54	5.60	6.55	6.9	10.8
Ce	14.19	14.29	16.48	13.5	21.3
Pr	2.09	2.10	2.45		
Nd	10.01	10.16	11.95	8.6	11.9
Sm	2.80	2.84	3.37	2.87	2.9
Eu	1.03	1.03	1.20	1.01	0.92
Gd	3.25	3.29	4.10		
Tb	0.54	0.54	0.68	0.67	0.61
Dy	3.35	3.35	4.42		
Ho	0.66	0.67	0.85		
Er	1.87	1.90	2.41		
Tm	0.28	0.28	0.36		
Yb	1.66	1.68	2.11	2.34	2.41
Lu	0.25	0.25	0.31	0.36	0.4
Th	0.67	0.60	0.69	1.0	1.68
U	0.37	0.24	0.27	0.7	0.8
Ta	0.30	0.23	0.25	0.42	0.53
Hf	2.05	2.27	2.48	2.01	2.32
Pb	2.19	2.65	2.65		
Cs				0.3	0.47
Co				61.4	39.3
Sc				35	37.4
$^{87}Sr/^{86}Sr$				0.70600	0.70564
± 2 SE				±2	±15
$^{87}Sr/^{86}Sr_{182}$	0.70579	0.70376	0.70355	0.70578	0.70527
$^{143}Nd/^{144}Nd$				0.512726	0.512505
± 2SE				±7	±8
$^{143}Nd/^{144}Nd_{182}$	0.512561	0.512551	0.512565	0.512475	0.512322
εNd_{190}	2.9	2.7	3.0	1.6	-1.5
$^{206}Pb/^{204}Pb$		18.21		18.474±7	18.781± 9
$^{207}Pb/^{204}Pb$		15.47		15.561±8	15.670±9
$^{208}Pb/^{204}Pb$		37.58		38.111±15	38.300±23

Table 2. Geochemical, mineralogical and petrographical characteristics of the different groups of Falkland Islands intrusions.

Type	**Type locality**	**Mitchell[1]**	**Stone[2]**	**Petrographic features**	**Mineralogy**	**Subgroup**	**Mg#**	**SiO_2**	**TiO_2**	**Ti/Zr**	**Zr/Y**	**$^{87}Sr/^{86}Sr_{182}$**	**εNd_{182}**
Dyke Island (DIT)	Dyke Island 51º59'33" S 60º52'50" W	Not defined	Radial swarm	Fine-grained aphyric, rarely plagioclase ± augite-phyric	Plag + Aug	Acid	<22	62-75	0.2-1.6	<31	5.0-8.8	0.7055-0.7098	-2.8 to -0.5
						Low TiO_2	27-57	52-61	1.1-1.7	24-67	4.8-7.4		
						High TiO_2	41-51	53-58	>1.80	25-53	6.8-8.4		
Port Sussex Creek (PST)	Port Sussex 51º40'15" S 58º58'41" W	N-S	NE-SW	Coarse-grained dolerite	Pig ± Opx + Aug Rare Ol + Di	none	48-58	52-54	0.9-1.2	50-70	3.6-5.3	0.7077 -0.7134	-5.5 to -10.9
E-W	Fox Bay West 51º57'02" S 60º05'21" W	E-W	E-W	Coarse-grained olivine dolerite	Ol + Plag ± Aug	none	42-64	47-54	1.0-1.9	77-90	3.2-4.8	0.7036-0.7058	-0.4 to +3.0
Mount Alice (MAT)	Mount Alice 52º09'12" S 60º35'55" W	Mount Alice	Radial swarm	Fine-grained plagioclase ± olivine phyric	Ol + Plag ± Aug	none	44-64	47-50	1.3-1.9	98-142	3.2-5.2	0.7031-0.7039	0.0 to +3.7
Lively Island (LI)	Lively Island 52º00'00" S 58º27'47" W	Lively Island	NE-SW	Coarse-grained with accessory biotite	Rare pigeonite	none	48-52	51-52	0.8-0.9	53	4.0-4.54	0.7053	-0.5 to -1.4

1. Groups described by Mitchell *et al*. (1999); 2. Groups defined by Stone *et al.* (2009)

Calculated extract for fractionation of PST and E-W intrusions

	PST			E-W		
	NGF16	MHF5.1	Calc	ECF12	ECF44	Calc
SiO_2	54.01	53.81	53.82	49.69	51.03	50.98
TiO_2	0.94	1.00	1.13	1.05	1.21	1.36
Al_2O_3	13.20	14.97	15.02	13.30	15.21	15.20
FeO	10.60	10.62	10.60	10.51	11.11	11.06
MnO	0.20	0.17	0.18	0.17	0.17	0.21
MgO	9.67	6.78	6.78	11.62	6.71	6.70
CaO	8.81	9.50	9.49	9.81	11.51	11.50
Na_2O	1.96	2.62	2.56	2.29	2.56	2.46
K_2O	0.48	0.42	0.56	0.32	0.39	0.39
P_2O_5	0.12	0.11	0.15	0.11	0.11	0.13
Extract			%			%
Olivine	Fo_{83}		0.0			57.0
Plagioclase	An_{70}		18.9			40.4
Orthopyroxene	$En_{71}Fs_{19}Wo_9$		74.7			
Clinopyroxene	$En_{51}Fs_{13}Wo_{33}$		6.4			2.6
Σ residuals^2			0.127			0.038
F			0.79			0.75

Table 4 AFC parameters for the trajectories shown in Fig. 12. R is the ratio of assimilated rock to crystal cumulate. A value appropriate for upper-crustal contamination has been used. F is the total amount of crystallization required to reach the most extreme composition on a particular trajectory. T_{CHUR} is the Chondritic Uniform Reservoir model Nd age for the most extreme composition on a particular trajectory, in Ga.

		AFC parameters								T_{CHUR}
		Sr	**Nd**	**εNd**	**$^{87}Sr/^{86}Sr$**	**D_{Sr}**	**D_{Nd}**	**R**	**F**	**(Ga)**
CT1	Source	50	5	2	0.7035	0.5	0.1	0.40	≤0.2	3.0
	Crust	400	20	-50	0.7120					
PST-1	Source	60	4	2	0.7035	0.5	0.1	0.40	≤0.2	2.2
	Crust	350	40	-20	0.7200					
PST-2	Source	100	5	2	0.7035	0.5	0.1	0.40	≤0.2	1.8
	Crust	350	60	-10	0.7250					